Available online at www.sciencedirect.com

ScienceDirect

Geochimica et Cosmochimica Acta 183 (2016) 198–233

Geochimica et Cosmochimica Acta

www.elsevier.com/locate/gca

Chemostratigraphy of the Sudbury impact basin fill: Volatile metal loss and post-impact evolution of a submarine impact basin

Edel M. O'Sullivan [a,*], Robbie Goodhue [a], Doreen E. Ames [b], Balz S. Kamber [a]

[a] Department of Geology, School of Natural Sciences, Trinity College Dublin, College Green, Dublin 2, Ireland
[b] Natural Resources Canada, Geological Survey of Canada, Ottawa, Canada

Received 20 November 2015; accepted in revised form 3 April 2016; Available online 8 April 2016

Abstract

The 1.85 Ga Sudbury structure provides a unique opportunity to study the sequence of events that occurred within a hydrothermally active subaqueous impact crater during the late stages of an impact and in its aftermath. Here we provide the first comprehensive chemostratigraphic study for the lower crater fill, represented by the ca. 1.4 km thick Onaping Formation. Carefully hand-picked ash-sized matrix of 81 samples was analysed for major elements, full trace elements and C isotopes.

In most general terms, the composition of the clast-free matrix resembles that of the underlying melt sheet. However, many elements show interesting chemostratigraphies. The high field strength element evolution clearly indicates that the crater rim remained intact during the deposition of the entire Onaping Formation, collapsing only at the transition to the overlying Onwatin Formation. An interesting feature is that several volatile metals (e.g., Pb, Sb) are depleted by >90% in the lower Onaping Formation, suggesting that the impact resulted in a net loss of at least some volatile species, supporting the idea of "impact erosion," whereby volatile elements were vaporised and lost to space during impact. Reduced C contents in the lower Onaping Formation are low (<0.1 wt%) but increase to 0.5–1 wt% up stratigraphy, where $\delta^{13}C$ becomes constant at −31‰, indicating a biogenic origin. Elevated Y/Ho and U/Th require that the ash interacted with saline water, most likely seawater. Redox-sensitive trace metal chemostratigraphies (e.g., V and Mo) suggest that the basin was anoxic and possibly euxinic and became inhabited by plankton, whose rain-down led to a reservoir effect in certain elements (e.g., Mo). This lasted until the crater rim was breached, the influx of fresh seawater promoting renewed productivity.

If the Sudbury basin is used as an analogue for the Hadean and Eoarchaean Earth, our findings suggest that hydrothermal systems, capable of producing volcanogenic massive sulphides, could develop within the rims of large to giant impact structures. These hydrothermal systems did not require mid-ocean ridges and implicitly, the operation of plate tectonics. Regardless of hydrothermal input, enclosed submarine impact basins also provided diverse isolated environments (potential future oases) for the establishment of life.

Keywords: Submarine impact; Hydrothermal environment; Sudbury; Volatile loss; Origin of life

1. INTRODUCTION

The role of large to giant meteorite impacts on terrestrial geology is an area of long-standing interest (e.g., Maher and Stevenson, 1988; Elkins-Tanton et al., 2004). One significant question concerns the flux of meteoritic material

* Corresponding author at: Institute of Geological Sciences, University of Bern, Baltzerstrasse 1+3, 3012 Bern, Switzerland. Tel.: +41 75 4175860.
E-mail address: osullied@tcd.ie (E.M. O'Sullivan).

http://dx.doi.org/10.1016/j.gca.2016.04.007
0016-7037/

brought to the Earth during the late phases of planetary accretion, particularly with respect to the platinum group elements (PGEs), which display highly distinctive chondritic signatures (e.g., Petrus et al., 2015a), and water, which is thought to have originated in part from extraterrestrial sources during all stages of planetary accretion (e.g., Morbidelli et al., 2000). Kimura et al. (1974) discovered a discrepancy between the absolute and relative abundances of siderophile elements in the Earth's mantle compared to experimental data regarding their sequestration into the metallic core. These authors proposed that a "late veneer" of meteoritic material was added to the upper mantle inventory of siderophile elements. This delivery could have occurred during the cataclysmic Late Heavy Bombardment between 4.0 and 3.8 Ga (Maier et al., 2009), in a relatively lower temperature and lower energy regime than earlier planetary accretion. It is therefore possible that these giant impactors also delivered volatile species, including water and carbon, both essential for the construction and evolution of our planet's hydrosphere and biosphere (e.g., Kleine, 2011).

A second area of interest concerning meteorite impacts is the evolution of life. Popular ideas for the origin of life centre around the chemical evolution and synthesis of organic molecules in subaqueous environments such as warm lakes or lagoons, or in particular in hydrothermal springs near mid ocean ridge systems (Lazcano et al., 1983; Baross and Hoffman, 1985). The discovery of "Lost City"-type hydrothermal systems, found several kilometres away from mid ocean ridges with ultramafic chemical compositions has promoted comparisons with the putative primordial ocean floor (e.g., Kelley et al., 2005). However, these systems too implicitly assume operation of plate spreading. The high hydrostatic pressure of subaqueous environments is favourable to the spontaneous synthesis of organic molecules, and excludes harmful solar or cosmic radiation (e.g., Daniel et al., 2006 and references therein). It has long been known that carbonaceous chondrites of the CI and CM group, and more recently comets (Goesmann et al., 2015), contain a variety of organic compounds (e.g., Cloëz, 1864) including glycine, β-alanine and γ-amino-n-butyric acid (Ehrenfreund et al., 2001). The influx of meteoritic material to the Earth during the late stages of planetary accretion possibly delivered both sufficient amounts of these essential building blocks and the energy necessary for the synthesis of complex organic molecules (e.g., Chyba et al., 1990). However, it has also been speculated that the energy delivered by giant impacts was sufficient to heat the atmosphere to a point that would sterilise the planet. For example, impactors 250 km in diameter could deliver enough energy to sterilise the entire planet including the deep oceans (Maher and Stevenson, 1988; Sleep et al., 1989). Recent investigations indicate that impact induced boiling and evaporation of the early oceans may have continued until at least as late as 3.25 Ga (Lowe and Byerly, 2015). It seems probable that the energy delivered from large (>65 km diameter) or giant (>250 km diameter) meteorite impacts would have eradicated life from at least the surface of the Earth repeatedly, only to be re-established in another location by the remnant extremophiles that survived the previous event (Maher and Stevenson, 1988; Abramov and Kring, 2004). Stüeken et al. (2013) discussed the difficulty of combining all the necessary factors for the synthesis of organic molecules into one single environment on the Hadean surface. In this context, the role of impact basins have remained underexplored, largely because of the paucity of such structures on the modern Earth surface.

In the existing literature, research has largely focused on the study of impact ejecta layers, deposited outside the impact structure. For example, most of the knowledge regarding the consequences of the Chicxulub impact event come from the study of time-equivalent sediments rather than from data of the buried structure itself (e.g., Alvarez et al., 1980) with only a few studying drill core data of the impact fill (e.g., Keller et al., 2004). Recently, Petrus et al. (2015a) presented the first detailed account of the distribution of meteoritic signatures within the crater fill of the ca. 1.85 Ga Sudbury structure. The current paper builds on the study of Petrus et al. (2015a) by providing the first comprehensive chemostratigraphic study for a large impact basin fill, for use as an analogue for the effects of Hadean impact events on the development of early life.

2. GEOLOGICAL SETTING AND RELEVANT PREVIOUS WORK

The roughly 60 km × 30 km Sudbury impact structure, Ontario, Canada, is a topic of long-standing controversy. Originally it was believed to be of igneous origin (e.g., Muir, 1984), due to the presence of the differentiated igneous body known as the Sudbury Igneous Complex (SIC), the evidence for the presence of hydrothermal activity (e.g., Ames et al., 1998, 2006), and many volcanic features in the immediate crater fill (e.g., Ames et al., 2002). However, more recent studies have led to the consensus (e.g., Grieve, 1994) that the structure is the remnant of an originally much larger circular multi-ring impact basin with a diameter of between 150 and 260 km (Pope et al., 2004). Structural comparison with the lunar crater classifications of Baker and Head (2013) suggests that the Sudbury structure may have originally resembled a protobasin or even a peak-ring basin depending on the unknown original size. Regardless of this classification, in this manuscript, the term 'crater' is used to refer to the geological structure generated by the meteorite impacts of any size, whereas the term 'basin' is used in a sedimentological sense, referring to the body of water hosted by the crater, creating an isolated depositional environment.

The impact occurred on the terrane boundary between the southernmost Superior Province and the Southern Province, dominated by granites, gneisses, metasediments and metavolcanics. The occurrence of carbonaceous clasts within the basin fill (Bunch et al., 1999) and the discovery of impact-generated surge deposits in the Gunflint Formation cherts (Addison et al., 2005, 2010) have supported the consensus that the target was subaqueous, possibly in the shallow foreland basin of the Penokean orogenic belt (e.g., Shanks and Schwerdtner, 1991). The remnant of the crater has been deformed into an ellipsoid-shaped syncline

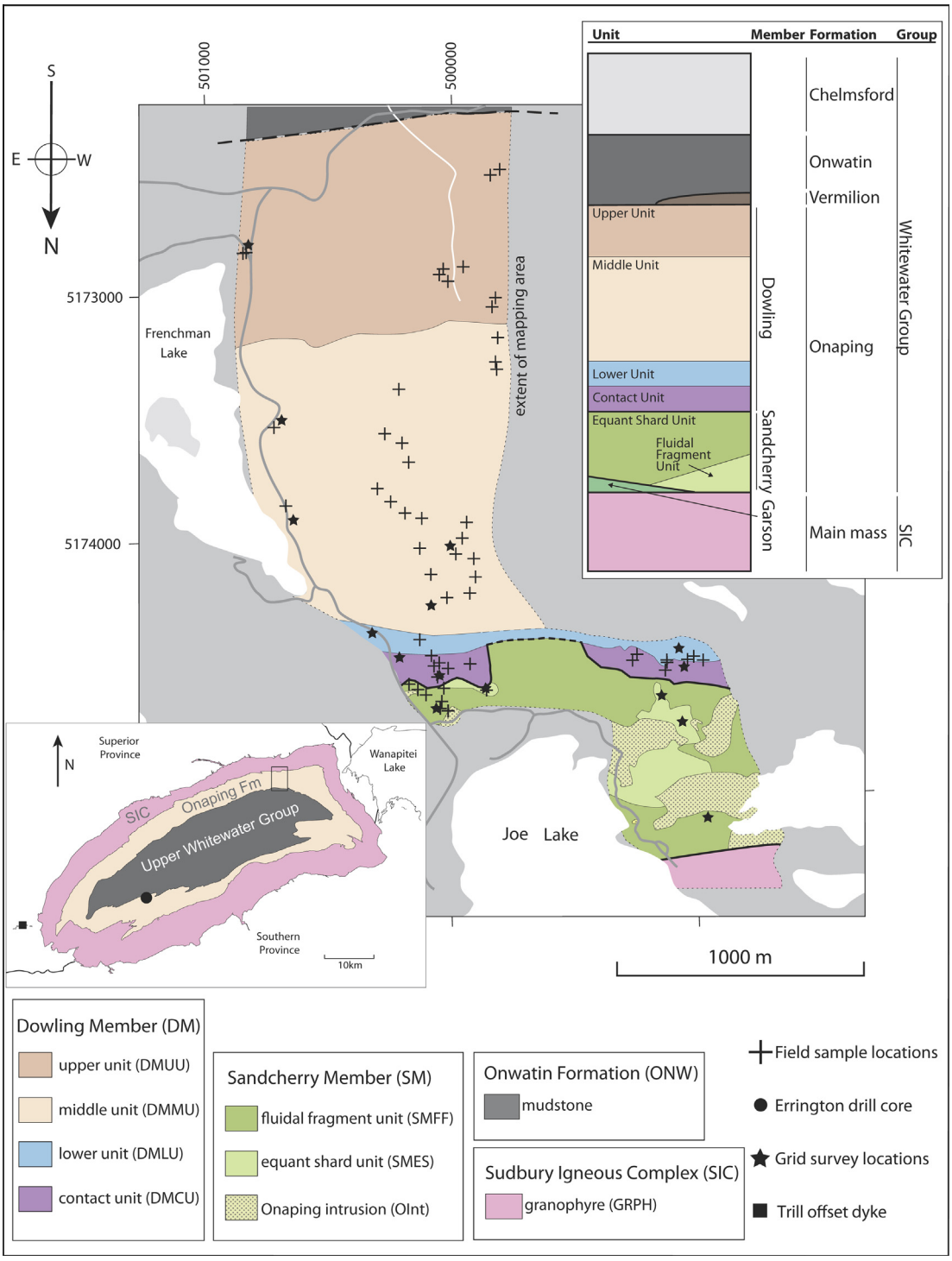

Fig. 1. Geological map of Joe Lake area showing Onaping Formation lithologies and Onwatin Formation. Field sampling locations are indicated with black crosses. Inset top right: General stratigraphy of Sudbury crater fill for clarity of unit sequence. Not to scale. Inset bottom left: general Sudbury structure showing Errington drill core ERR-13-210 location as a black circle. Map is inverted for clarity of the stratigraphic sequence, the granophyre being the lowermost unit in the stratigraphy and the Onwatin Formation the highest. *Map sources:* This study, Ames and Gibson (2004).

during the Penokean Orogeny and subsequent deformation events (e.g., Hirt et al., 1993, Fig. 1). The geometry of the syncline and the quality of the outcrops revealed by erosion during subsequent glaciations provide a unique opportunity to study the post-impact processes that affected the crater by exposing the entire stratigraphy of the crater fill

(Fig. 1). The structure comprises shock-deformed footwall, the melt sheet and the basin fill. The melt sheet differentiated into basal mafic to felsic norite units, middle quartz gabbro, and upper granophyre, with radiating dykes intruding into the footwall rocks known as "offset dykes". The melt sheet and the dykes collectively compose the SIC. Directly above the SIC lies the Whitewater Group, comprising the impact crater fill.

The Whitewater Group is divided into four formations: (1) The Onaping Formation, which was deposited directly on top of the SIC. It is divided (from bottom to top) into a sparsely preserved Garson Member (0–500 m thick) comprised of quartzite block-rich megabreccia and breccia units, and is overlain by a consistently developed ca. 1400 km complex series of breccias and tuffs, separated into the Sandcherry Member and the Dowling Member (Gibbins, 1994; Ames et al., 1998, 2006). The Sandcherry Member is mainly composed of breccias of fragmented and shock melted target rocks and limited ash matrix, whereas the younger, more voluminous Dowling Member is composed of lenticular devitrified glass shards, small lithic clasts, and an increasing proportion of ash matrix. The Sandcherry–Dowling Member contact is characterised by faulting and collapse units associated with the initial modification of the crater structure (Ames, 1999; Ames et al., 2000); (2) The thin (~14 m), laterally discontinuous Vermilion Formation, composed of carbonate rocks, siltstones and turbidites hosting 6.4 Mt of Zn–Pb–Cu deposits (Ames et al., 2002, 2006; Rousell and Brown, 2009); (3) The Onwatin Formation, a ~600 m thick sequence of carbonaceous shales; and (4) the Chelmsford Formation, consisting of post-impact greywacke turbidites and sandstones (Ames, 1999).

The Onaping Formation has several enigmatic features. Most significantly, its 1400 m thickness is inconsistent with an origin as a fallback breccia (as originally proposed, e.g. by Grieve et al. (1991)). Other recognised impact structures (Grieve et al., 2010), results of experimental models (Collins et al., 2005) and observations from lunar impact craters (Spudis et al., 2014) predict much thinner fallback breccias, leaving the source of the excess material in the Onaping Formation unexplained. The unexpectedly thick impact fill has drawn much attention previously, prompting explanations such as impact-induced tsunami wash-in and post-impact sedimentation (Peredery and Morrison, 1984). Furthermore, abundant reduced C is homogenously distributed within the ash matrix, but is absent from the lithic fragments and volcanic clasts, yielding the distinctive dark colour of the surrounding matrix (Supplemental Fig. 1A, B). The occurrence of significant amounts of reduced C in high-temperature volcaniclastic rocks is elsewhere restricted to much more recent formations, such as the Cretaceous-Palaeocene Nuussuaq hyaloclastites and tuffs (Dam et al., 2009). There, coal deposits and oil seepage within the volcaniclastics resulted from the deposition of largely terrestrial and shallow marine sediments. Although the Nuussuaq hyaloclastites invite an interesting qualitative comparison, it must be noted that the Sudbury basin predates the emergence of land organisms by more than 1 Ga, emphasising the unusual circumstances of the occurrence of reduced C in the Onaping Formation.

It was first speculated by Gibbins (1994) that the Onaping Formation was not a fallback breccia, but was instead produced by the violent interaction of water with an unknown source of magma. This proposal overcame the significant problem of explaining the volcanogenic characteristics of the Onaping Formation in the context of the impact event proposed by Dietz (1964). The melt–water interaction mechanism has since been adopted by the impact community (e.g., Grieve et al., 2010; Stöffler et al., 2013). Most recently, evidence of hydroclastic fracturing of magmatic material has been extended to the upper Dowling Member, suggesting that explosive volcanic activity persisted throughout deposition of the entire Onaping Formation (Ames et al., 2002). Continued production of volcanic material would likely have contributed to the excessive thickness of the Onaping Formation. Presently, the Onaping Formation has not been dated directly, and so estimates of the lifespan of this activity rely on computational modelling and simulation. A model for the timing and extent of heat loss and crystallisation from the SIC proposed by Abramov and Kring (2004) suggests that the melt sheet would have reached liquidus temperatures by 4000 years after the impact event, and would have solidified within 20,000 years. However, deeper-seated magma sources may have driven hydrothermal activity until up to 200,000 years following the impact. The system is predicted to have returned to normal geothermal gradients by 2 Ma after impact, apart from isolated heat flows that may not have reached the surface.

Many studies of the Onaping Formation have focused on the changes in physical characteristics and petrographical evidence in comparison to other studied impact craters (e.g., French, 1970; Grieve et al., 2010), but relatively few studied its geochemistry (e.g., Ames et al., 2002; Mungall et al., 2004). Dressler et al. (1996) compiled trace element data from earlier studies (e.g., Muir and Peredery, 1984) with their own analysis of 15 recrystallized glass fragments for comparison with the putative impact melt of the SIC. Their vitric clasts were highly variable in composition and supported the view of vitrification of individual melt pods from heterogeneous target material. Ames et al. (2002) presented the first modern trace element analysis of the Onaping Formation and the vitric components. Their data suggested that the composition of the impact melt remained constant throughout the deposition of the entire Onaping Formation, with elevated high field strength elements (HFSEs) relative to the SIC and a complex genetic relationship between the vitric component and the SIC. Subsequently, Mungall et al. (2004) investigated the crustal contributions to the impact melt by analysing the concentration of PGE's in the Onaping Formation matrix. Their clast-free samples showed Ir and Ru anomalies that could only be accounted for by either a mantle contribution to the impact melt, or from the impactor itself. Most recently, Petrus et al. (2015a) revisited the PGE elevation by analysing the siderophile and a few lithophile element signatures of 69 samples of Onaping Formation matrix to show that

PGE concentrations were best explained by contribution from a comet with a chondritic refractory component.

This study, for the first time, builds on the previous stratigraphic volcanological and facies work by constructing a comprehensive multi-element and isotope chemostratigraphy – a tool that is now commonly applied to sedimentary sequences and volcanic provinces. Whitehead et al. (1990) had already found interesting C and S abundance and isotope trends across a short stratigraphic interval, encompassing the upper 100 m of the Dowling Member and lowest 50 m of the Onwatin Formation. Their data revealed largely biogenic values between ~−29.9‰ and ~−22.9‰ for the reduced C of the upper Onaping Formation, accompanied by fluctuating trends in the C/S ratio. They also demonstrated a change in chemical composition through the contact with the Onwatin Formation, and suggested that environmental conditions fluctuated between biogenic and hydrothermal sulphide deposition.

The aims of the present study were to: (1) revisit the unresolved issue of heterogeneous vs. homogeneous composition of the matrix; (2) extend the study of the Onaping–Onwatin Formation boundary to the lithophile elements; (3) search for geochemical evidence for melt–seawater interaction; and (4) tie the C-isotope record to the chemostratigraphy of redox-sensitive metals.

3. METHODOLOGY

3.1. Field work

Field work was carried out during three separate field campaigns in 2012, 2013 and 2014. Samples from the 2014 campaign were collected by the first author whereas samples of the 2012 and 2013 campaigns were collected by Joseph Petrus (Laurentian University) and Gavin Kenny (Trinity College Dublin).

3.1.1. Grid surveys

Initial inspection of the components of the Onaping Formation on a broad scale was carried out by conducting 15 quantitative grid surveys along two transects at Joe Lake during the 2014 field campaign (Fig. 1; Supplemental Fig. 2A). Changes in abundance, size and shape of each component of the breccias and tuffs across all units of the Sandcherry Member and the Dowling Member were quantified by placing a 1 × 1 m grid on relatively fresh, lichen-free outcrops for point-counting. One hundred samples were categorised in a representative area of each unit. Classified components included lithic fragments, fluidal fragments, devitrified green glass ("green shards"), argillites, and ash matrix. Also noted were petrology of lithic fragments, presence or absence of vesicles in devitrified glass shards and presence or absence of melt rims.

3.1.2. Outcrop sample collection

Ash matrix samples were taken in the North Range to avoid complications arising from more advanced deformation experienced by the South Range. The units were distinguished by the configuration of clasts in the outcrop as outlined by Ames and Gibson (2004). Unweathered samples were systematically collected with a sledge hammer along a transect through each unit of the Onaping Formation to the west and south of Joe Lake, perpendicular to the contact between the Onaping Formation and the SIC (Fig. 1). Areas of strong weathering and pervasive alteration earlier described by Ames et al. (2004) were avoided. Samples were collected from the top of the Sandcherry Member and the entire Dowling Member at approximately 50–80 m intervals. Outcrop paucity and difficult terrain in the Middle and Upper Units limited the continuity of the transect in these areas. It should be noted that the resolution of the geochemical dataset is restricted to a precision of 50–80 m, in a single location. However, a compilation of detailed geologic maps of the entire Sudbury structure by Ames and Gibson (2004) revealed a highly symmetrical structure, with the exception of the discontinuous and irregular Contact Unit of the Dowling Member, and the higher intensity of deformation in the South Range compared to the North Range. The Contact Unit was deliberately over-proportionally sampled on account of its interesting petrology.

3.1.3. Drill core sample collection

Outcrops of the Onaping–Onwatin Formation contact are extremely sparse and available exposures are invariably badly weathered, rendering them unsuitable for geochemical analysis. Fresh samples of the uppermost unit of the Dowling Member-Onwatin Formation transition were instead obtained from a ~250 m drill core (ERR-13-210) recovered at the Errington Mine area in the South Range in December 2013 (Fig. 1; Supplemental Fig. 2C), courtesy of Glencore mining company. As is usual for the Onaping Formation–Onwatin Formation contact, strata in the core experienced localised folding and overturning. Samples were collected from a segment containing the complete sequence from the uppermost unit of the Dowling Member into the Onwatin Formation, separated by the thin sulphide deposits of the Vermilion Formation. The section was evidently overturned, though experienced only limited internal deformation. Samples were systematically collected and described at approximately 10 m intervals in the Dowling Member, increasing to 4 m intervals approaching the contact, and finally collected at 1 m intervals within the Onwatin Formation. The thin (1.5 m) Vermilion Formation was also collected in its entirety but not analysed for this study.

3.2. Sample preparation

Samples chosen for analysis from the 2013 and 2014 field campaigns were selected on the basis of distribution along the transect, extent of weathering and minimal amount of visible secondary sulphides. Thin sections of 131 samples were prepared to assess the extent of alteration in candidate samples, and to provide a petrographic supplement to the chemostratigraphy (Supplemental Fig. 1A–C). The whole rock samples were split and crushed using a jaw crusher. The crush was washed and then diligently hand-picked in alcohol under a microscope to separate matrix, avoiding lithic clasts in order to isolate the chemical signal of the ash-sized component (Supplemental Fig. 2D).

Individual matrix fragments ranged in size from 300–500 μm in the matrix-poor, lithic fragment-rich Sandcherry Member and lower Dowling Member, to 500–2000 μm in the middle and upper Dowling Member. Weathered surfaces, sawn edges and altered material were avoided. Clean separation was more challenging in the Sandcherry Member samples due to the limited amount of ash matrix. The hand-picked samples were then hand-milled and homogenised in an agate mortar. Samples from the 2012 field campaign were prepared in a similar manner at Laurentian University, Sudbury. The powdered samples were divided up for each analytical technique. During matrix separation, fine-grained, laminated argillite clasts were found in a few samples of the lower and middle units of the Dowling Member. These argillite samples warranted separate examination as black shales were absent from known target rocks at the time of impact, and a few argillites were hand-picked separately for analysis.

Samples for stable isotope analysis were decalcified to remove carbonate. 200 mg aliquots of powdered samples were placed in micro-tubes, dried in an oven at 50 °C overnight, and then weighed. Approximately 2 ml of 0.5 M HCl was pipetted into each micro-tube to completely submerge the sample and placed in the oven at 50 °C for 6 h until effervescence ceased. The samples were then centrifuged for 30 s each and the acid was removed using a pipette. Purified water was added to each sample and shaken vigorously, centrifuged and removed by pipette three times to remove any remaining HCl. The samples were again dried overnight in an oven at 50 °C and then weighed to record total loss. This process was repeated once more to ensure all carbonate material was removed.

3.3. Major and trace elements

Small (200 mg) aliquots of each ash matrix sample were reserved for major element analysis using a Spectro Arcos ICP-OES. Samples were ignited in ceramic crucibles in an oven at 1100 °C for 1 h and subsequently weighed to record loss on ignition. Lithium metaborate flux (0.8 g) was then added to 0.1 g ignited sample and heated to 1100 °C for 20 min until fused. The melt bead was dissolved in 100 g 5% HNO_3 + Y internal standard, and transferred into polystyrene beakers. A 2.5 g aliquot of stock solution was further diluted with 5% HNO_3 to a dilution factor of 13,000 for analysis. Standards W-2, BIR-1, BHVO-2, JA-3, AVG-2 and SCO-1 were used for instrument calibration and quality control.

Trace element analyses were obtained with a Thermo SCIENTIFIC iCAP Q ICP-MS at Trinity College Dublin from a separate 100 mg unignited powder aliquot. Analytical procedures and instrument operation followed those of Babechuk et al. (2010).

Enrichment factors (EFs) for elements Mo, U and V were calculated after Algeo and Tribovillard (2009) for comparison to modern restricted basin environments. EF were calculated as $X_{EF} = [(X/Al)_{sample}/(X/Al)_{PAAS}]$, where X and Al represent weight concentrations of elements X and Al, respectively.

3.4. C isotopes

Decalcified samples were analysed for $\delta^{13}C_{org}$ in reduced carbon and wt%C_{org} using a Thermo DeltaPlus CF-EA-IRMS. Samples were weighed into tin capsules and placed into a tray with 20 L-alanine standards. Required sample masses were calculated and weighed accordingly to give peak signals of between 1500 mV and 6000 mV. Sample weights ranged from ~40 mg in the reduced C-poor samples of the Sandcherry Member to ~4 mg in the Upper Unit of the Dowling Member and ~1.5 mg for samples of the C-rich Onwatin Formation. The $\delta^{13}C_{org}$ of the 75 samples were corrected to the VPDB Primary Standard using IEAE-CO-1 and IAEA-CO-9 and yielded a precision of 0.07‰.

4. RESULTS

4.1. Major elements

Major element and loss on ignition (LOI) data are listed in Table 1. Major element data would typically be used for rock classification on a total alkali vs silica (TAS) diagram for volcanogenic rocks but the main purpose in this study was to calculate the chemical index of alteration (CIA), calculated as $Al_2O_3/[Al_2O_3 + CaO^* + Na_2O + K_2O] \times 100$ (Nesbitt and Young, 1982), and plotted on an Al_2O–$(CaO^* + Na_2O)$–K_2O (A–CN–K) ternary diagram (Fig. 2, Fedo et al., 1995). Results show that the matrix of the Sandcherry Member and the Contact and Lower Units of the Dowling Member largely plot within a CIA range of 40–70. Samples collected from the drill core show a CIA range from 60–100. This confirms the microscopic observation that the material in the uppermost Dowling Member and Onwatin Formation experienced more advanced weathering with the expected trend for argillites. Regardless of the relatively low CIA values of the Sandcherry Member and lower Dowling Member samples, lithophile elements such as Na, K and Si in ash particles may nonetheless have been affected by geochemical reactions in the subaqueous environment, and thus interpretation of these data must be treated with caution. Nonetheless, the average SiO_2 content of 62.5 ± 1.6% in the Onaping Formation matrix is comparable to the average SiO_2 content of the SIC calculated by Therriault et al. (2002) of 64.6% (for comparison, both were calculated to a total of 98.3 wt% anhydrous species and 1.7% LOI). Average Al_2O_3 content of 11.3 ± 1.1% in the Onaping Formation is also similar to that of the SIC, at 13.8%.

4.2. Trace elements

Trace element data for all samples are listed in Table 1. The 2012 field campaign data were reported in Petrus et al. (2015a) and interpreted within the context of meteorite origin.

4.2.1. Lithophile elements

The HFSEs are widely regarded as some of the least mobile and most refractory of the lithophile elements. A

Table 1
Major element (wt%), total organic carbon (wt%) and loss on ignition (wt%), trace element (ppm) and carbon isotope data. Ti trace element data presented in wt%.

Sample	12JAP-072	12JAP-029	WM-15	12JAP-022	13GGK043	13GGK078	13GGK077	12JAP-069	13GGK076	12JAP-068	12JAP-121	12JAP-067	13GGK059	12JAP-122
Stratigraphic height	266	288			248	273	298	305	310	327	332	347	384	293
Lithology	ABOMB	ADIKE	QD	QD	SMES	SMES	SMES	SMES	SMES	SMES	SMES	SMES	SMES	SMFF
SiO_2[a]				60.5	61.7			59.6		65.0	67.1			59.8
TiO_2				0.68	0.54			0.75		0.49	0.50			0.60
Al_2O_3				14.6	12.1			12.6		11.8	11.8			13.8
Fe_2O_3				7.26	8.93			10.2		6.15	5.78			8.23
MnO				0.13	0.14			0.22		0.17	0.13			0.13
MgO				3.83	4.87			5.26		3.88	3.27			4.67
CaO				5.45	3.95			3.51		3.59	2.54			2.61
Na_2O				3.30	4.72			3.10		4.52	3.62			3.61
K_2O				2.30	1.70			2.94		2.19	3.10			3.42
P_2O_5				0.21	0.17			0.21		0.15	0.13			0.18
LOI				1.83	1.25			1.84		2.13	2.10			3.14
Total				100.11	100.04			100.18		100.04	100.10			100.21
CIA				52.8	47.2			55.9		51.6	56.0			58.8
Cwt%[b]					0.01	0.01	0.01	0.04	0.01	0.06	0.07	0.11	0.01	0.04
$\delta^{13}C$[c]					−26.5	−26.8	−26.9	−26.3	−27.9	−26.4	−27.4	−29.4	−27.4	−25.8
Li	4.11	4.67	26.6	25.5	11.2	7.45	15.8	17.0	7.53	7.02	10.6	17.2	2.42	18.1
Be	0.89	1.33	1.31	1.33	1.66	1.88	2.64	1.58	1.95	1.44	1.15	1.49	1.41	1.55
Sc	13.6	10.9	17.2	17.5	17.2	17.8	16.9	18.1	19.6	13.1	12.9	13.9	10.0	17.1
Ti[d]	NQ	NQ	0.42	0.43	0.37	0.31	0.27	0.47	0.25	0.30	NQ	0.33	0.23	0.38
V[d]	56.1	NQ	131	134	152	165	184	153	187	118	95.7	123	132	134
Cr	111	101	143	151	125	137	134	159	157	109	123	117	86.0	139
Co	14.0	13.7	69.5	26.5	23.2	24.7	19.9	35.0	19.8	13.5	18.3	21.7	12.5	35.4
Ni	23.1	50.0	72.9	74.9	69.1	67.9	79.9	96.2	61.4	49.7	56.9	64.2	32.3	55.6
Cu	1.30	16.2	58.8	59.5	3.40	3.65	2.07	22.1	1.57	15.6	44.4	31.5	1.45	0.38
Zn[e]	15.0	18.7	76.0	75.6	BDL	BDL	BDL	40.4	BDL	19.6	24.5	21.3	19.8	23.7
Ga	14.6	12.2	18.0	18.3	18.9	15.3	17.8	25.7	12.3	13.2	12.9	15.3	9.84	19.8
As	0.44	0.36	1.94	0.84	0.43	1.47	0.97	0.97	1.40	0.60	1.35	2.15	0.52	5.38
Rb[d]	NQ	NQ	88.2	85.5	45.0	21.8	4.28	85.6	6.31	67.1	NQ	66.2	120	112
Sr	53.3	68.9	375	384	53.7	61.2	39.3	78.0	44.2	107	163	172	46.2	126
Y	13.0	13.1	18.5	18.8	19.7	21.3	21.4	22.1	22.6	15.8	16.0	17.0	14.4	18.0
Zr	106	133	164	169	142	145	130	208	129	135	131	143	90.2	156
Nb	6.47	6.40	8.28	8.10	8.33	8.58	9.33	11.4	8.72	7.76	7.26	8.20	6.07	7.91
Mo	0.39	1.63	1.17	1.23	17.5	0.67	2.37	5.34	1.51	5.65	3.60	5.14	7.49	3.63
Ag[f]	0.06	0.10	0.17	0.16	0.03	0.02	0.13	0.12	0.02	0.10	0.08	0.12	0.02	0.08
Cd	0.07	0.07	0.11	0.11	0.04	0.04	0.04	0.07	0.10	0.06	0.05	0.08	0.04	0.06
In	0.02	0.02	0.05	0.05	0.06	0.06	0.09	0.03	0.08	0.06	0.03	0.04	0.11	0.05
Sn	0.38	0.32	1.41	1.40	1.86	1.65	4.89	0.74	3.09	3.77	0.93	1.48	1.67	0.51

(*continued on next page*)

Table 1 (*continued*)

Sample	12JAP-072	12JAP-029	WM-15	12JAP-022	13GGK043	13GGK078	13GGK077	12JAP-069	13GGK076	12JAP-068	12JAP-121	12JAP-067	13GGK059	12JAP-122
Stratigraphic height	266	288			248	273	298	305	310	327	332	347	384	293
Lithology	ABOMB	ADIKE	QD	QD	SMES	SMES	SMES	SMES	SMES	SMES	SMES	SMES	SMES	SMFF
Sb	0.06	0.08	0.08	0.09	0.08	0.09	0.08	0.13	0.09	0.16	0.15	0.19	0.05	0.10
Cs	0.38	0.25	2.26	2.23	0.13	0.09	0.12	0.29	0.05	0.22	0.34	0.33	0.19	0.31
Ba[d]	NQ	693	658	672	358	255	41.2	1010	67.4	733	1260	733	974	1430
La	10.2	20.1	36.0	36.7	70.7	21.9	29.7	22.1	37.3	29.5	25.0	31.5	49.6	14.0
Ce[d]	21.6	41.3	74.0	75.2	125	47.1	64.1	47.0	67.5	61.0	NQ	64.9	86.8	35.6
Pr	2.81	4.77	8.51	8.66	12.6	5.96	7.78	5.69	7.19	6.90	6.11	7.36	8.90	4.84
Nd	11.3	17.6	31.2	31.9	40.2	24.0	29.3	23.2	24.6	25.1	22.5	26.7	28.4	19.6
Sm	2.45	3.35	5.58	5.64	6.04	5.52	5.99	5.29	4.98	4.49	4.17	4.81	4.31	4.05
Eu	0.31	0.73	1.36	1.36	1.05	1.01	1.03	0.98	0.99	1.32	0.63	1.12	0.58	0.69
Gd	2.35	2.82	4.50	4.56	4.55	4.72	4.94	4.39	4.50	3.53	3.44	3.84	3.31	3.56
Tb	0.38	0.42	0.64	0.65	0.62	0.67	0.70	0.62	0.68	0.51	0.51	0.56	0.45	0.53
Dy	2.32	2.42	3.55	3.65	3.64	3.88	4.04	3.73	4.04	2.86	2.92	3.13	2.65	3.09
Ho	0.48	0.50	0.71	0.73	0.75	0.79	0.82	0.80	0.83	0.59	0.60	0.64	0.54	0.66
Er	1.32	1.40	1.96	1.99	2.05	2.19	2.31	2.28	2.29	1.61	1.70	1.74	1.46	1.89
Tm	0.19	0.21	0.29	0.29	0.31	0.33	0.35	0.34	0.34	0.24	0.25	0.26	0.22	0.29
Yb	1.19	1.34	1.83	1.87	1.92	2.07	2.31	2.11	2.11	1.51	1.62	1.64	1.36	1.88
Lu	0.17	0.20	0.27	0.27	0.29	0.31	0.36	0.31	0.30	0.23	0.24	0.24	0.20	0.29
Hf	2.86	3.30	4.02	4.10	3.56	3.69	3.26	5.20	3.32	3.36	3.34	3.56	2.24	3.91
Ta	0.57	0.45	3.17	0.50	0.54	0.61	0.51	0.72	0.63	0.52	0.53	0.55	0.40	0.53
W	0.15	0.14	144	0.33	0.36	2.18	2.09	0.68	1.29	1.03	0.76	0.71	0.82	0.30
Tl	1.07	0.46	0.58	0.55	0.23	0.11	0.02	0.42	0.03	0.33	0.47	0.34	0.57	0.61
Pb	2.81	2.70	12.2	10.3	0.81	0.43	0.52	1.44	0.71	1.38	2.04	3.18	0.34	0.96
Th	11.6	7.08	7.86	7.92	7.16	7.79	8.50	13.8	4.49	7.54	8.55	8.31	4.49	8.44
U	3.22	2.53	1.71	1.73	3.67	3.67	5.88	5.20	3.91	3.06	3.38	3.22	2.13	3.19
Nb/Ta	11.28	14.08	2.61	16.26	15.45	14.06	18.34	15.88	13.83	14.97	13.70	15.00	15.11	14.85
Zr/Hf	37.04	40.41	40.90	41.23	39.83	39.33	39.81	40.00	38.83	40.14	39.24	40.21	40.32	40.01
Nb/Th	0.558	0.904	1.053	1.023	1.164	1.100	1.098	0.824	1.943	1.030	0.849	0.987	1.351	0.938
Y/Ho	27.11	26.40	25.99	25.83	26.41	26.87	26.03	27.49	27.14	26.82	26.56	26.58	26.95	27.28
U/Th	0.277	0.357	0.217	0.219	0.513	0.471	0.692	0.376	0.872	0.406	0.396	0.388	0.475	0.379

Sample	12JAP-108	13GGK014	13GGK027	12JAP-003	12JAP-066	13GGK030	13GGK031	13GGK052	13GGK048	12JAP-064	13GGK015	13GGK016	13GGK061	14PCG088	14PCG089
Stratigraphic height	375	362	370	373	380	388	398	411	415	453	375	378	383	457	486
Lithology	SMFF	DMCU	DMCU	DMCU	DMCU	DMCU	DMCU	DMCU	DMCU	DMCU	DMLU	DMLU	DMLU	DMLU	DMLU
SiO_2	62.6			61.8	61.3					62.7	63.7			61.0	62.7
TiO_2	0.64			0.52	0.53					0.56	0.48			0.43	0.41
Al_2O_3	13.5			11.8	12.1					12.4	10.5			12.2	12.8
Fe_2O_3	6.96			8.96	7.93					8.07	8.05			7.25	5.83
MnO	0.15			0.18	0.12					0.13	0.19			0.23	0.25

MgO	4.37			4.63	5.64					5.77	4.86			4.25	3.87
CaO	3.01			3.99	2.19					2.34	4.88			5.76	5.58
Na_2O	3.34			3.69	3.93					3.95	3.68			2.69	3.53
K_2O	4.95			2.16	1.06					1.07	1.74			2.69	2.91
P_2O_5	0.19			0.16	0.17					0.17	0.14			0.14	0.13
LOI	0.37			2.36	6.33					2.49	1.93			3.78	2.12
Total	100.07			100.19	101.35					99.65	100.13			100.37	100.16
CIA	47.4			54.5	61.4					61.9	46.6			58.4	48.0
Cwt%[a]	0.03	0.01	0.03	0.04	0.06	0.01	0.02	0.01	0.10	0.29	0.12	0.11	0.18	0.61	0.60
$\delta^{13}C$[b]	−24.8	−27.7	−28.3	−27.4	−26.9	−26.2	−27.9	−27.7	−27.4	−30.8	−29.8	−29.6	−30.8	−31.2	−31.3
Li	11.3	12.6	6.74	14.2	27.6	8.61	10.0	8.93	8.30	14.9	10.0	10.6	7.21	10.6	6.96
Be	1.52	1.84	1.59	1.47	1.22	1.43	1.79	1.58	1.32	1.20	1.52	1.39	1.32	1.39	1.53
Sc	15.7	17.5	14.1	13.5	14.5	15.5	15.9	16.6	13.1	12.4	14.8	15.1	13.1	13.0	12.4
Ti	NQ	0.35	0.29	0.32	0.34	0.31	0.34	0.35	0.35	NQ	0.31	0.33	0.31	0.27	0.25
V	NQ	174	140	135	139	131	138	143	145	NQ	148	143	134	134	116
Cr	129	127	87.1	131	128	106	105	117	93.7	113	99.8	96.7	96.1	84.3	73.8
Co	21.3	26.4	16.3	20.6	19.7	19.3	13.4	17.9	15.3	18.2	17.0	17.7	13.9	18.1	12.2
Ni	67.4	79.3	53.3	67.2	55.5	58.2	35.8	46.5	48.5	72.2	53.3	48.4	50.4	62.3	43.5
Cu	16.1	2.23	3.22	8.39	20.4	22.7	5.95	17.5	26.2	30.2	9.0	12.7	17.1	43.8	18.0
Zn	43.7	BDL	25.0	25.8	14.5	BDL	BDL	BDL	16.5	44.1	BDL	28.8	26.5	50.7	27.0
Ga	17.4	15.9	10.9	14.5	15.7	13.4	16.9	14.5	14.5	15.7	13.2	16.0	12.6	13.4	11.8
As	0.52	1.14	0.57	0.68	0.36	0.37	0.70	0.61	0.47	0.99	2.11	1.17	0.42	4.72	1.49
Rb	NQ	30.9	31.7	64.1	25.0	80.6	76.1	63.6	57.8	53.6	49.0	62.4	60.9	72.7	81.7
Sr	107	44.4	42.3	73.5	90.6	132	169	98.2	154	153	93.3	131	100	179	167
Y	18.9	19.1	14.5	17.3	18.0	18.1	18.0	19.5	16.4	17.2	17.1	16.6	15.5	17.4	15.6
Zr	179	128	106	136	147	137	151	149	115	128	118	116	116	105	102
Nb	8.76	9.11	8.10	8.49	9.05	9.16	8.59	9.42	8.68	8.18	8.42	8.95	8.53	7.88	7.31
Mo	4.33	2.15	3.46	7.69	7.88	4.59	5.14	5.29	3.08	7.76	6.15	5.91	6.49	10.6	7.73
Ag	0.10	0.03	0.04	0.10	0.10	0.03	0.02	0.08	0.02	0.09	0.06	0.13	0.03	NA	NA
Cd	0.08	0.07	0.05	0.06	0.06	0.05	0.04	0.05	0.03	0.06	0.11	0.04	0.04	0.03	0.03
In	0.03	0.05	0.04	0.07	0.04	0.04	0.04	0.04	0.04	0.04	0.03	0.05	0.04	0.04	0.04
Sn	0.70	2.68	2.54	2.31	1.38	3.44	3.18	3.19	2.74	1.31	3.08	3.16	3.30	1.26	1.27
Sb	0.10	0.20	0.13	0.32	0.10	0.24	0.36	0.14	0.14	0.20	0.23	0.26	0.25	1.18	0.84
Cs	0.44	0.12	0.10	0.26	0.34	0.32	0.32	0.19	0.33	0.71	0.21	0.23	0.20	0.39	0.29
Ba	NQ	292	295	567	272	694	628	687	655	433	452	592	543	751	916
La	15.4	33.0	22.0	30.2	32.5	29.4	45.0	62.0	28.0	26.5	36.6	31.3	25.4	31.8	31.1
Ce	38.4	60.3	44.5	60.6	66.4	58.8	88.4	119	56.9	NQ	73.4	62.6	51.4	67.4	66.2
Pr	5.21	7.07	5.39	6.91	7.56	7.02	10.0	13.6	6.72	6.42	8.37	7.22	5.96	7.35	7.25
Nd	20.8	26.1	19.5	25.4	27.5	26.5	35.3	48.3	24.7	23.7	29.6	26.3	21.8	26.8	26.5
Sm	4.06	4.54	3.77	4.54	5.00	5.08	5.76	7.11	4.44	4.60	4.92	4.70	3.92	4.76	4.70
Eu	0.65	0.99	0.84	1.16	1.21	1.11	1.24	1.37	0.98	1.24	1.01	1.06	0.85	1.07	1.06
Gd	3.47	3.91	3.21	3.79	4.08	4.30	4.32	4.93	3.68	3.92	3.81	3.76	3.21	3.92	3.76
Tb	0.53	0.59	0.46	0.55	0.59	0.61	0.57	0.62	0.53	0.57	0.53	0.53	0.46	0.53	0.50
Dy	3.13	3.55	2.69	3.13	3.31	3.48	3.33	3.65	3.08	3.16	3.10	3.10	2.75	3.14	2.89
Ho	0.67	0.72	0.54	0.64	0.67	0.69	0.67	0.73	0.61	0.64	0.63	0.63	0.57	0.64	0.58

(*continued on next page*)

Table 1 (*continued*)

Sample	12JAP-108	13GGK014	13GGK027	12JAP-003	12JAP-066	13GGK030	13GGK031	13GGK052	13GGK048	12JAP-064	13GGK015	13GGK016	13GGK061	14PCG088	14PCG089
Stratigraphic height	375	362	370	373	380	388	398	411	415	453	375	378	383	457	486
Lithology	SMFF	DMCU	DMCU	DMCU	DMCU	DMCU	DMCU	DMCU	DMCU	DMCU	DMLU	DMLU	DMLU	DMLU	DMLU
Er	1.94	1.90	1.45	1.77	1.82	1.83	1.82	1.98	1.64	1.71	1.73	1.67	1.58	1.70	1.53
Tm	0.29	0.27	0.21	0.26	0.27	0.26	0.26	0.29	0.23	0.25	0.25	0.24	0.23	0.24	0.22
Yb	1.87	1.62	1.33	1.66	1.70	1.62	1.64	1.82	1.44	1.58	1.53	1.44	1.41	1.48	1.40
Lu	0.28	0.24	0.20	0.24	0.25	0.24	0.24	0.27	0.21	0.23	0.23	0.21	0.21	0.22	0.21
Hf	4.47	3.27	2.71	3.37	3.70	3.41	3.77	3.70	2.91	3.22	3.00	3.00	2.93	2.67	2.58
Ta	0.58	0.49	0.51	0.55	0.58	0.54	0.59	0.61	0.56	0.53	0.54	0.57	0.55	0.51	0.47
W	0.41	0.78	0.40	0.54	0.53	1.25	2.14	1.95	0.95	0.52	0.91	1.30	0.52	1.07	1.10
Tl	0.84	0.18	0.17	0.36	0.14	0.46	0.42	0.32	0.32	0.33	0.28	0.34	0.34	0.45	0.54
Pb	6.09	1.28	0.78	2.84	3.43	1.61	2.77	5.00	2.00	7.07	3.19	2.11	2.02	4.88	4.65
Th	10.2	5.33	7.25	7.81	7.56	7.13	9.93	8.14	7.41	7.14	8.43	7.53	7.54	6.52	6.34
U	3.57	2.83	2.63	3.67	3.89	2.72	3.30	3.36	3.21	3.82	3.55	3.26	3.23	4.08	3.52
Nb/Ta	15.14	18.47	15.90	15.42	15.55	16.91	14.57	15.45	15.38	15.56	15.57	15.78	15.62	15.39	15.64
Zr/Hf	40.06	39.08	39.06	40.31	39.68	40.04	40.16	40.21	39.40	39.79	39.35	38.68	39.47	39.37	39.40
Nb/Th	0.856	1.709	1.118	1.087	1.196	1.284	0.865	1.158	1.172	1.146	0.998	1.187	1.131	1.208	1.153
Y/Ho	28.15	26.53	26.91	26.89	26.92	26.21	26.78	26.81	26.85	27.05	27.03	26.55	27.15	27.38	27.10
U/Th	0.349	0.531	0.363	0.470	0.514	0.381	0.332	0.413	0.433	0.535	0.422	0.433	0.428	0.626	0.555

Sample	12JAP-063	14PCG090	14PCG091	14PCG091ARG	12JAP-062	14PCG092	14PCG093	14PCG093ARG	12JAP-061	12JAP-060	12JAP-059	13GGK008	12JAP-058	14PCG100
Stratigraphic height	500	521	534	534	552	562	591	591	608	622	646	661	674	717
Lithology	DMLU	DMLU	DMLU	DMLU-ARG	DMMU	DMMU	DMMU	DMMU-ARG	DMMU	DMMU	DMMU	DMMU	DMMU	DMMU
SiO_2	64.0	67.7			62.4	62.1	62.7		62.4	63.7	61.4	61.9	62.5	62.0
TiO_2	0.48	0.37			0.51	0.36	0.38		0.47	0.45	0.46	0.49	0.42	0.42
Al_2O_3	11.4	13.1			12.0	12.9	11.0		10.7	10.5	10.6	11.0	10.5	11.2
Fe_2O_3	7.06	3.78			9.11	4.61	6.24		8.98	8.22	8.45	8.52	8.58	6.47
MnO	0.23	0.13			0.22	0.19	0.29		0.32	0.39	0.35	0.34	0.38	0.29
MgO	5.04	2.31			5.52	2.75	3.17		5.14	4.81	4.09	4.61	4.63	3.28
CaO	4.56	3.45			2.67	4.13	5.80		3.97	4.93	5.02	3.63	4.98	6.28
Na_2O	2.90	2.69			2.77	2.35	1.79		1.75	2.06	2.13	1.76	2.07	2.10
K_2O	1.55	4.86			1.12	4.61	2.93		1.42	2.18	2.38	2.27	2.78	2.34
P_2O_5	0.15	0.11			0.16	0.11	0.14		0.17	0.15	0.16	0.15	0.14	0.14
LOI	3.04	1.72			4.41	6.10	6.54		4.94	2.68	5.75	5.68	3.17	6.36
Total	100.43	100.22			100.87	100.24	100.99		100.22	100.12	100.70	100.38	100.12	100.91
CIA	60.9	52.8			67.6	59.3	64.2		70.7	56.4	63.4	67.3	57.4	65.2
Cwt%[a]	0.58	0.58	0.69		0.42	0.54	0.63		0.32	0.35	0.38	0.61	0.39	0.80
$\delta^{13}C$[b]	−31.5	−31.3	−31.1		−31.1	−29.8	−29.9		−30.4	−31.9	−30.7	−30.3	−31.0	−30.8
Li	18.6	4.69	5.42	3.47	27.6	16.8	14.8	7.40	22.5	13.7	16.3	23.3	9.62	15.0

Be	1.45	0.90	1.10	0.75	1.20	1.30	1.25	0.97	1.50	1.90	1.46	1.43	1.62	1.21
Sc	13.1	9.29	12.4	6.28	13.5	11.0	10.5	6.70	12.3	11.7	11.7	12.0	11.1	10.3
Ti	0.32	0.21	0.23	0.24	0.32	0.27	0.25	0.17	0.29	0.28	0.28	0.31	0.26	0.26
V	144	69.3	90.9	29.3	137	98.3	93.0	48.5	128	124	117	132	117	92.4
Cr	106	59.1	67.3	66.4	117	79.9	82.2	55.9	120	108	104	101	112	78.9
Co	16.3	17.7	19.2	10.3	22.0	14.5	14.2	16.1	20.6	17.2	18.4	13.0	16.3	13.0
Ni	59.9	28.4	35.9	20.9	65.4	49.6	52.9	58.8	66.0	63.1	63.1	42.4	55.6	45.5
Cu	39.2	12.3	22.8	12.9	198	19.2	21.2	73.6	56.1	37.5	38.4	17.4	30.2	17.0
Zn	52.5	22.9	37.9	12.6	51.6	39.4	39.7	36.1	70.8	49.8	49.4	BDL	61.6	42.3
Ga	13.9	9.75	10.5	10.6	15.2	11.0	10.6	7.75	14.0	12.8	12.4	14.6	12.0	10.6
As	0.81	25.0	24.1	14.2	1.29	8.36	3.42	3.89	0.48	0.76	4.81	3.53	2.96	8.16
Rb	38.0	143	145	219	27.5	59.6	65.0	59.5	34.5	58.7	65.2	50.5	71.7	47.2
Sr	143	174	183	186	119	105	100	94.1	164	179	120	86.2	161	97.6
Y	17.1	13.0	13.7	6.99	17.5	15.9	14.3	10.8	17.2	16.6	16.4	15.9	15.3	14.7
Zr	126	91.5	104	99.0	137	120	112	79.1	142	129	133	121	125	114
Nb	8.36	6.12	6.75	6.92	8.78	8.26	7.71	5.22	9.04	8.48	8.45	8.85	7.93	8.04
Mo	6.88	5.53	6.09	0.71	6.59	6.16	5.99	3.92	6.29	5.98	5.03	5.53	5.26	5.30
Ag	0.13	NA	NA	0.13	0.20	NA	NA	0.30	0.14	0.10	0.13	0.11	0.10	NA
Cd	0.07	0.04	0.06	0.04	0.08	0.06	0.06	0.08	0.10	0.06	0.06	0.14	0.09	0.07
In	0.04	0.03	0.03	0.01	0.04	0.02	0.02	0.02	0.04	0.04	0.03	0.03	0.03	0.02
Sn	1.37	1.08	1.14	0.82	1.46	1.00	0.84	0.68	1.24	1.42	1.12	2.41	1.00	1.15
Sb	0.85	0.62	0.78	0.28	0.53	0.23	0.37	0.42	0.56	0.60	0.59	0.35	0.71	0.28
Cs	0.41	0.43	0.44	0.78	0.34	0.30	0.31	0.31	0.27	0.31	0.32	0.38	0.31	0.25
Ba	473	1440	1690	1880	446	815	941	847	644	823	853	742	1220	848
La	29.7	30.2	30.1	6.77	29.8	23.6	22.7	18.3	28.7	28.5	27.5	22.4	25.6	20.3
Ce	65.2	62.7	62.5	18.0	61.1	50.6	47.4	33.7	58.3	58.4	56.2	46.3	52.2	44.3
Pr	6.92	6.70	6.69	2.40	6.98	5.53	5.11	3.69	6.66	6.58	6.34	5.45	5.91	4.98
Nd	25.1	24.1	24.1	9.10	25.5	20.4	18.9	13.3	24.3	23.9	23.5	20.4	21.5	18.7
Sm	4.62	4.09	4.12	1.71	4.67	3.77	3.47	2.50	4.43	4.35	4.29	3.84	3.91	3.55
Eu	1.11	0.98	0.83	0.27	1.08	0.83	0.77	0.53	1.05	1.04	0.96	0.80	0.88	0.81
Gd	3.79	3.24	3.28	1.45	3.81	3.25	2.95	2.20	3.65	3.55	3.51	3.30	3.25	3.05
Tb	0.55	0.43	0.44	0.21	0.57	0.46	0.42	0.32	0.54	0.52	0.51	0.47	0.47	0.44
Dy	3.06	2.47	2.55	1.26	3.20	2.72	2.44	1.87	3.05	2.97	2.94	2.80	2.70	2.55
Ho	0.63	0.49	0.51	0.26	0.65	0.57	0.51	0.38	0.63	0.61	0.60	0.57	0.56	0.53
Er	1.72	1.27	1.37	0.75	1.79	1.56	1.42	1.04	1.74	1.66	1.64	1.60	1.55	1.47
Tm	0.26	0.18	0.20	0.12	0.27	0.23	0.21	0.15	0.26	0.25	0.25	0.23	0.24	0.21
Yb	1.61	1.09	1.23	0.76	1.68	1.44	1.32	0.94	1.63	1.57	1.55	1.48	1.47	1.35
Lu	0.24	0.16	0.18	0.12	0.25	0.21	0.20	0.14	0.24	0.23	0.23	0.22	0.22	0.20
Hf	3.19	2.29	2.65	2.67	3.46	2.99	2.76	2.08	3.47	3.22	3.32	3.06	3.07	2.82
Ta	0.55	0.42	0.46	0.57	0.58	0.51	0.48	0.37	0.56	0.55	0.53	0.55	0.50	0.50
W	0.60	1.49	1.35	0.71	0.72	1.18	1.22	0.51	0.76	0.69	0.75	0.86	0.73	1.01
Tl	0.26	0.92	0.91	1.36	0.21	0.44	0.48	0.44	0.23	0.40	0.45	0.35	0.52	0.39
Pb	6.19	3.30	3.81	7.17	3.61	4.93	4.84	8.39	4.93	4.19	3.80	6.31	3.50	5.74
Th	7.20	5.93	6.56	10.5	7.55	7.00	6.65	5.54	7.56	7.23	6.65	7.00	6.64	6.32
U	3.74	2.78	2.92	1.77	3.84	4.62	3.32	2.90	3.89	3.72	3.55	3.29	3.33	3.11

(*continued on next page*)

Table 1 (*continued*)

Sample	12JAP-063	14PCG090	14PCG091	14PCG091ARG	12JAP-062	14PCG092	14PCG093	14PCG093ARG	12JAP-061	12JAP-060	12JAP-059	13GGK008	12JAP-058	14PCG100
Stratigraphic height	500	521	534	534	552	562	591	591	608	622	646	661	674	717
Lithology	DMLU	DMLU	DMLU	DMLU-ARG	DMMU	DMMU	DMMU	DMMU-ARG	DMMU	DMMU	DMMU	DMMU	DMMU	DMMU
Nb/Ta	15.30	14.62	14.80	12.20	15.24	16.16	16.20	14.21	16.11	15.54	15.81	16.04	15.96	16.17
Zr/Hf	39.63	40.02	39.15	37.05	39.65	40.17	40.43	38.13	40.84	39.99	40.08	39.55	40.64	40.37
Nb/Th	1.161	1.031	1.029	0.659	1.163	1.179	1.159	0.943	1.196	1.172	1.272	1.264	1.194	1.271
Y/Ho	27.05	26.77	26.75	26.68	26.69	28.02	28.00	28.11	27.16	27.31	27.28	27.66	27.25	27.62
U/Th	0.519	0.468	0.445	0.169	0.509	0.659	0.499	0.523	0.515	0.514	0.534	0.470	0.501	0.491

Sample	14PCG101	14PCG101ARG	12JAP-057	12JAP-037	12JAP-056	12JAP-095	12JAP-096	12JAP-099	12JAP-087	12JAP-091	12JAP-089	14PCG116	14PCG115	13GGK009
Stratigraphic height	755	755	776	818	857	966	980	1025	1065	1101	1074	1085	1142	1146
Lithology	DMMU	DMMU-ARG	DMMU	DMMU	DMMU	DMMU	DMMU	DMMU	DMMU	DMMU	DMUU	DMUU	DMUU	DMUU
SiO_2	64.0		62.7	62.1	63.4	63.3	62.8	63.2	61.7	64.0	62.3	62.4	59.6	61.8
TiO_2	0.43		0.44	0.45	0.40	0.45	0.45	0.43	0.44	0.43	0.47	0.54	0.44	0.46
Al_2O_3	11.5		10.2	10.8	8.95	10.5	10.1	10.1	10.2	10.1	10.8	10.6	11.2	10.2
Fe_2O_3	5.89		7.54	8.81	6.85	7.82	8.24	7.65	8.48	8.14	8.72	6.39	9.33	9.08
MnO	0.29		0.35	0.42	0.34	0.29	0.33	0.32	0.35	0.32	0.43	0.31	0.38	0.47
MgO	3.17		3.99	4.59	3.67	4.06	3.98	4.11	4.13	4.06	5.43	3.10	4.78	4.43
CaO	4.93		4.59	3.59	5.30	3.75	3.68	4.47	4.52	4.15	1.77	6.26	4.73	4.65
Na_2O	2.06		1.85	1.92	1.40	1.92	1.66	1.63	1.50	1.55	1.38	1.77	1.16	1.20
K_2O	2.81		1.92	3.52	1.93	2.20	2.02	2.31	2.21	2.41	2.45	2.75	2.39	2.08
P_2O_5	0.13		0.15	0.16	0.13	0.15	0.16	0.16	0.15	0.16	0.17	0.14	0.15	0.21
LOI	5.84		7.18	4.20	7.51	6.47	6.38	7.26	7.10	5.95	5.75	6.81	6.90	5.93
Total	101.00		100.96	100.63	99.84	100.95	99.87	101.64	100.74	101.32	99.63	101.11	101.07	100.51
CIA	64.0		66.6	60.8	67.1	65.5	67.3	66.2	67.6	66.3	68.7	64.4	71.4	70.8
Cwt%[a]	0.63		0.45		0.52	0.68	0.63	0.71	0.50	0.76	0.41	0.61	0.66	0.58
$\delta^{13}C$[2]	−30.3		−29.9		−30.9	−30.0	−30.0	−29.8	−29.8	−29.9	−29.3	−30.6	−30.9	−30.7
Li	14.5	8.30	16.4	9.70	15.3	18.2	19.3	19.5	22.1	20.2	28.5	16.7	27.9	21.9
Be	1.30	0.79	1.34	1.63	1.39	1.29	1.38	1.41	1.27	1.29	1.27	1.10	1.46	1.57
Sc	10.8	5.88	10.7	11.3	9.67	12.2	11.0	10.2	11.5	10.6	11.4	8.98	11.4	11.8
Ti	0.27	0.17	NQ	0.27	0.24	0.28	0.28	NQ	NQ	NQ	0.28	0.27	0.28	0.29
V	91.3	51.0	NQ	117	102	105	120	NQ	NQ	NQ	121	85.6	162	127
Cr	80.5	50.4	101	113	90.2	95.5	107	98.8	101	91.8	105	78.9	93.3	100
Co	12.7	7.37	16.2	17.8	14.2	14.9	16.4	14.9	17.9	15.0	20.1	13.0	18.1	15.3
Ni	36.1	26.0	56.5	66.0	51.9	55.9	62.5	51.5	61.4	56.5	62.7	38.9	60.8	48.8
Cu	6.60	9.66	18.1	39.4	19.6	25.0	21.6	14.8	38.6	24.8	39.6	7.65	45.9	21.2
Zn	39.3	28.6	55.1	60.5	51.6	57.3	89.3	54.5	118	72.7	96.4	38.9	67.4	BDL
Ga	10.5	9.04	11.9	12.8	11.1	12.1	12.9	12.1	12.4	12.2	12.9	10.2	14.2	13.5
As	10.3	5.79	7.88	0.46	5.91	5.52	6.00	4.87	3.48	5.05	5.60	13.4	0.55	3.31

Rb	51.1	122	41.2	76.4	41.0	48.6	46.7	46.8	40.3	45.6	46.8	50.9	43.0	43.8
Sr	82.9	96.9	78.6	94.7	90.0	82.2	76.1	92.7	87.3	82.9	61.1	101	75.9	86.7
Y	14.5	8.83	14.8	16.0	14.0	15.4	16.1	14.7	14.4	15.0	15.8	14.2	16.9	17.8
Zr	108	102	122	127	110	127	134	131	126	121	137	113	148	139
Nb	8.28	5.29	7.79	8.43	7.19	8.60	8.65	8.19	8.33	8.34	8.76	7.05	9.81	9.43
Mo	3.90	1.63	4.09	5.75	4.55	4.37	4.92	4.86	4.42	4.39	3.81	4.16	4.70	4.76
Ag	NA	0.40	0.19	0.21	0.17	0.12	0.12	0.12	0.14	0.13	0.12	NA	NA	0.04
Cd	0.08	0.08	0.17	0.13	0.17	0.10	0.11	0.10	0.23	0.12	0.13	0.06	0.06	0.05
In	0.02	0.01	0.03	0.03	0.02	0.02	0.03	0.02	0.03	0.03	0.03	0.02	0.03	0.03
Sn	0.92	0.51	1.03	1.11	0.88	1.44	0.90	1.12	0.79	1.71	1.07	0.49	0.83	2.52
Sb	0.21	0.17	0.22	0.70	0.29	0.30	0.32	0.37	0.35	0.46	0.39	0.29	0.30	0.42
Cs	0.26	0.55	0.25	0.33	0.27	0.49	0.54	0.42	0.35	0.37	0.50	0.34	0.44	0.32
Ba	1090	1790	1110	1420	707	1040	965	NQ	NQ	NQ	1100	1060	835	708
La	23.1	12.0	23.9	26.3	22.6	27.1	26.5	25.0	25.2	24.5	27.3	25.5	27.3	28.8
Ce	49.8	24.6	NQ	54.4	46.3	NQ	53.5	NQ	NQ	NQ	55.6	53.9	58.7	57.0
Pr	5.46	2.92	5.71	6.18	5.23	6.17	6.12	5.73	5.80	5.80	6.32	5.88	6.36	6.59
Nd	20.2	10.9	21.0	22.5	19.2	22.5	22.3	20.8	21.1	21.3	23.0	21.4	23.2	24.2
Sm	3.67	2.10	3.85	4.08	3.49	4.03	4.06	3.75	3.73	3.85	4.12	3.76	4.05	4.33
Eu	0.77	0.38	0.90	0.97	0.79	0.85	0.87	0.66	0.73	0.81	0.87	0.76	0.93	0.93
Gd	3.12	1.80	3.20	3.42	2.96	3.28	3.38	3.10	3.06	3.16	3.35	3.07	3.44	3.66
Tb	0.44	0.26	0.47	0.50	0.43	0.48	0.50	0.45	0.45	0.46	0.48	0.42	0.47	0.51
Dy	2.55	1.56	2.69	2.87	2.47	2.71	2.82	2.56	2.56	2.64	2.77	2.46	2.75	3.01
Ho	0.52	0.33	0.55	0.58	0.50	0.56	0.58	0.53	0.53	0.54	0.57	0.51	0.58	0.63
Er	1.44	0.91	1.50	1.61	1.38	1.55	1.63	1.50	1.50	1.51	1.60	1.40	1.61	1.75
Tm	0.21	0.14	0.23	0.24	0.21	0.23	0.24	0.22	0.22	0.22	0.24	0.21	0.24	0.26
Yb	1.31	0.87	1.41	1.50	1.29	1.45	1.53	1.40	1.42	1.41	1.50	1.31	1.52	1.59
Lu	0.19	0.13	0.21	0.22	0.19	0.22	0.23	0.21	0.21	0.21	0.22	0.20	0.23	0.24
Hf	2.69	2.66	3.04	3.15	2.72	3.18	3.38	3.28	3.18	3.07	3.41	2.77	3.56	3.42
Ta	0.51	0.42	0.50	0.53	0.46	0.54	0.55	0.52	0.52	0.52	0.54	0.48	0.59	0.57
W	1.06	0.76	0.70	0.67	0.55	1.06	0.56	0.91	0.65	1.84	0.76	0.71	0.85	0.92
Tl	0.41	0.88	0.33	0.58	0.31	0.39	0.39	0.40	0.34	0.40	0.41	0.45	0.37	0.46
Pb	3.72	6.44	14.8	6.39	7.87	4.91	5.26	5.19	6.42	4.63	10.8	5.91	4.01	5.38
Th	6.47	6.82	6.70	7.03	5.77	6.64	7.17	7.04	7.22	6.68	7.17	6.11	7.05	7.19
U	2.91	1.56	3.08	3.57	2.98	3.33	3.51	3.34	3.36	3.33	3.36	2.94	4.32	4.47
Nb/Ta	16.35	12.56	15.63	15.85	15.70	15.98	15.63	15.84	16.05	16.08	16.25	14.72	16.75	16.56
Zr/Hf	40.11	38.22	40.33	40.26	40.38	39.81	39.79	39.91	39.72	39.49	40.04	40.70	41.51	40.72
Nb/Th	1.279	0.776	1.162	1.198	1.245	1.295	1.206	1.165	1.154	1.249	1.221	1.153	1.391	1.311
Y/Ho	27.72	27.12	26.82	27.51	27.87	27.54	27.65	27.47	26.83	27.53	27.70	27.80	29.20	28.33
U/Th	0.449	0.229	0.459	0.507	0.516	0.501	0.489	0.475	0.466	0.499	0.468	0.481	0.612	0.621
Sample	12JAP-038	14PCG114	12JAP-101	14PCG113	14EOS001	14EOS004	14EOS007	14EOS010	14EOS013	14EOS016	14EOS019	14EOS025	14EOS028	14EOS031
Stratigraphic height	1147	1166	1334	1343	1134	1161	1188	1217	1244	1259	1266	1287	1296	1304
Lithology	DMUU	DMUU	DMUU	DMUU	DMUU	DMUU	DMUU	DMUU	DMUU	DMUU	DMUU	DMUU	DMUU	DMUU
SiO_2	61.7	60.7	62.0	61.2	58.9	59.9	59.0	55.7	55.7	54.2	57.8	52.7	54.9	57.5
TiO_2	0.44	0.45	0.56	0.39	0.52	0.47	0.49	0.48	0.45	0.55	0.43	0.40	0.54	0.54

(*continued on next page*)

Table 1 (*continued*)

Sample	12JAP-038	14PCG114	12JAP-101	14PCG113	14EOS001	14EOS004	14EOS007	14EOS010	14EOS013	14EOS016	14EOS019	14EOS025	14EOS028	14EOS031
Stratigraphic height	1147	1166	1334	1343	1134	1161	1188	1217	1244	1259	1266	1287	1296	1304
Lithology	DMUU	DMUU	DMUU	DMUU	DMUU	DMUU	DMUU	DMUU	DMUU	DMUU	DMUU	DMUU	DMUU	DMUU
Al_2O_3	10.2	11.5	10.3	11.1	11.3	10.7	10.1	10.3	10.2	11.7	9.28	7.77	11.9	11.6
Fe_2O_3	8.72	8.49	8.09	7.49	10.3	10.9	11.4	13.1	16.1	12.5	6.86	8.74	13.4	10.6
MnO	0.44	0.36	0.27	0.28	0.20	0.27	0.42	0.45	0.40	0.32	0.73	1.22	0.39	0.51
MgO	4.24	4.18	3.44	3.66	4.60	6.03	4.95	8.77	6.92	11.6	4.60	8.55	10.5	8.76
CaO	4.67	4.71	4.42	5.50	1.96	2.19	2.97	1.80	1.52	0.99	6.14	6.78	0.39	1.74
Na_2O	1.38	1.61	1.60	1.73	0.11	0.04	0.04	BDL	BDL	BDL	0.03	BDL	BDL	BDL
K_2O	2.05	2.51	2.54	2.39	2.56	1.50	2.35	0.94	0.56	0.10	2.60	0.80	0.12	1.02
P_2O_5	0.16	0.16	0.15	0.13	0.22	0.19	0.20	0.21	0.20	0.20	0.18	0.14	0.20	0.22
LOI	6.67	6.17	7.08	6.69	10.1	8.60	9.15	9.48	9.07	8.91	13.8	14.6	8.60	8.64
Total	100.71	100.82	100.39	100.58	100.79	100.77	101.05	101.28	101.05	101.10	102.42	101.71	100.94	101.09
CIA	69.5	68.1	65.6	67.1	79.3	86.4	79.4	91.0	94.4	99.1	76.4	89.9	98.9	91.3
Cwt%[a]	0.29	0.53	0.67	0.61	3.37		2.57	2.95	2.53	2.18		2.59	2.72	2.16
$\delta^{13}C$[b]	−31.6	−30.3	−29.2	−30.1	−29.5		−29.6	−29.8	−29.1	−28.8		−22.1	−30.3	−28.7
Li	20.0	22.8	20.8	22.5	29.9	31.8	23.6	30.4	38.8	47.1	27.5	27.0	38.5	41.2
Be	1.42	1.44	1.19	1.26	1.69	1.53	1.42	0.68	1.31	0.83	1.79	1.35	0.69	1.89
Sc	10.7	11.3	10.9	10.7	10.8	11.4	12.3	10.6	9.91	12.4	9.16	8.41	11.1	10.7
Ti	0.27	0.27	0.26	0.25	0.31	0.29	0.29	0.29	0.29	0.35	0.26	0.21	0.32	0.33
V	114	117	109	109	269	209	236	251	246	263	214	187	275	244
Cr	102	93.7	93.0	85.9	91.0	88.3	81.2	83.8	82.0	110	73.7	63.6	100	101
Co	17.4	14.4	12.0	13.5	6.95	9.78	9.28	10.3	14.5	11.0	2.27	10.0	5.13	3.48
Ni	61.2	56.2	47.2	46.5	45.6	43.5	52.3	63.4	84.1	70.7	8.92	43.4	30.6	22.8
Cu	30.4	16.3	21.1	29.5	28.0	16.3	39.7	21.0	4.36	45.6	272	4.28	14.1	1.90
Zn	81.3	86.0	56.3	47.5	79.1	99.3	105	249	172	223	39.3	108	521	129
Ga	12.2	13.5	12.0	12.1	14.6	13.7	12.5	13.8	13.1	15.8	11.9	10.3	16.0	15.2
As	3.13	3.06	3.55	8.03	0.77	6.90	0.38	2.49	11.7	11.2	1.10	21.4	0.52	0.77
Rb	42.4	43.4	51.8	46.0	71.1	27.2	41.9	25.0	35.3	3.92	93.2	30.6	5.06	35.4
Sr	84.5	77.7	122	126	68.2	52.6	85.7	75.2	61.3	56.6	315	428	24.7	96.3
Y	16.0	15.2	14.9	14.5	18.2	14.2	15.9	14.5	18.8	20.5	16.8	13.5	16.2	18.9
Zr	135	134	126	120	130	126	116	122	110	153	108	94.1	141	140
Nb	8.57	9.16	8.64	8.32	16.3	12.1	14.3	14.9	14.8	15.5	14.0	9.85	14.9	17.0
Mo	3.55	4.83	3.84	3.34	31.2	17.5	26.2	25.3	26.4	22.4	23.3	17.6	22.7	24.0
Ag	0.12	NQ	0.13	NA	NA	NA	NA	NA	NA	NA	NA	NA	NA	NA
Cd	0.11	0.40	0.07	0.05	0.16	0.08	0.25	0.30	0.07	0.35	0.07	0.09	0.82	0.09
In	0.03	0.02	0.02	0.02	0.45	0.03	0.04	0.03	0.02	0.03	0.04	0.01	0.01	0.01
Sn	1.09	1.00	0.99	0.85	1.75	1.32	1.76	1.22	1.54	0.79	1.41	0.94	0.71	1.42
Sb	0.48	0.52	0.49	0.45	0.73	0.45	0.79	0.47	0.60	1.08	0.73	0.76	3.92	4.38
Cs	0.29	0.44	0.43	0.37	2.81	0.85	1.28	1.14	4.27	0.42	3.19	1.35	0.33	1.10
Ba	707	857	903	779	1540	1260	2260	441	80.4	19.3	1450	512	92.6	858

La	25.6	26.3	23.4	22.0	33.5	23.9	23.2	33.2	26.9	33.3	27.5	22.9	32.9	37.3
Ce	53.3	56.1	49.2	47.2	70.2	50.2	48.7	69.7	57.2	69.6	58.1	48.4	69.7	75.9
Pr	5.99	6.08	5.50	5.22	7.64	5.44	5.30	7.58	6.22	7.53	6.32	5.21	7.58	8.18
Nd	22.0	22.2	20.1	19.3	28.1	19.9	19.6	27.7	22.8	27.6	23.3	19.1	27.9	29.9
Sm	3.98	3.98	3.68	3.48	4.95	3.62	3.61	4.74	4.12	4.94	4.18	3.49	4.95	5.28
Eu	0.94	0.86	0.80	0.77	0.93	0.69	0.61	0.94	0.89	0.84	0.89	0.49	0.77	0.91
Gd	3.34	3.29	3.05	2.98	3.97	3.04	3.20	3.61	3.58	4.10	3.50	2.99	3.88	4.21
Tb	0.49	0.45	0.45	0.42	0.52	0.42	0.46	0.44	0.50	0.55	0.47	0.40	0.48	0.55
Dy	2.82	2.67	2.59	2.48	2.95	2.40	2.70	2.44	2.95	3.23	2.71	2.22	2.65	3.18
Ho	0.58	0.55	0.54	0.51	0.61	0.50	0.56	0.50	0.63	0.68	0.56	0.45	0.54	0.64
Er	1.61	1.51	1.49	1.43	1.72	1.42	1.59	1.42	1.73	1.92	1.57	1.24	1.56	1.80
Tm	0.24	0.23	0.22	0.21	0.26	0.22	0.24	0.22	0.25	0.29	0.23	0.18	0.24	0.27
Yb	1.49	1.43	1.40	1.33	1.63	1.39	1.53	1.41	1.54	1.83	1.48	1.18	1.56	1.67
Lu	0.22	0.22	0.21	0.20	0.25	0.21	0.23	0.22	0.23	0.28	0.22	0.18	0.24	0.25
Hf	3.30	3.31	3.14	2.91	3.25	3.11	2.88	3.01	2.73	3.68	2.68	2.32	3.46	3.41
Ta	0.53	0.55	0.52	0.50	0.95	0.75	0.86	0.90	0.87	0.88	0.80	0.62	0.86	0.94
W	0.43	1.01	0.60	0.71	2.69	1.34	1.68	1.20	0.47	2.26	2.13	1.90	3.02	3.33
Tl	0.35	0.38	0.44	0.42	1.20	0.41	0.73	0.51	0.83	0.11	1.47	0.74	0.13	0.65
Pb	7.12	3.82	17.5	8.17	10.4	8.78	4.49	7.94	3.18	42.9	41.1	7.86	50.7	165
Th	6.60	7.97	6.54	5.89	8.14	7.06	7.43	7.96	6.95	8.59	6.70	5.57	8.04	8.40
U	3.43	3.48	3.17	3.06	9.95	6.78	9.78	10.6	7.33	8.63	8.63	6.78	8.73	9.67
Nb/Ta	16.28	16.53	16.68	16.71	17.12	16.09	16.50	16.44	16.96	17.55	17.38	15.84	17.34	18.13
Zr/Hf	40.77	40.39	39.98	41.11	39.91	40.44	40.21	40.56	40.42	41.65	40.20	40.59	40.80	41.10
Nb/Th	1.299	1.150	1.321	1.412	2.007	1.712	1.919	1.867	2.126	1.807	2.086	1.767	1.852	2.020
Y/Ho	27.70	27.69	27.62	28.11	29.94	28.71	28.27	29.06	30.00	30.17	30.22	30.11	29.97	29.42
U/Th	0.519	0.437	0.485	0.520	1.223	0.961	1.316	1.327	1.055	1.005	1.288	1.215	1.085	1.151

Sample	14EOS034	14EOS037	14EOS040	14EOS048	14EOS050	14EOS054	14EOS057	14EOS060	14EOS063	14EOS066
Stratigraphic height	1315	1324	1335	1343	1346	1349	1354	1359	1364	1369
Lithology	DMUU	DMUU	DMUU	ONW	ONW	ONW	ONW	ONW	ONW	ONW
SiO_2	66.4	57.5	56.4	57.9	60.2	49.3	49.3	48.8	60.1	
TiO_2	0.47	0.48	0.42	0.67	0.46	0.87	0.93	1.01	0.59	
Al_2O_3	10.4	10.8	10.9	16.9	13.6	21.7	21.3	21.3	15.9	
Fe_2O_3	5.88	9.07	9.25	5.75	3.82	5.11	3.74	7.45	4.37	
MnO	0.54	0.53	0.50	0.05	0.45	0.10	0.15	0.11	0.14	
MgO	3.22	4.06	4.93	1.25	1.65	1.83	1.77	1.72	1.28	
CaO	3.35	4.75	5.08	0.43	3.41	0.95	1.33	1.05	1.30	
Na_2O	0.05	0.04	0.09	2.08	2.87	1.83	1.64	1.08	1.57	
K_2O	2.82	2.50	2.30	5.26	3.00	6.86	6.43	6.50	4.26	
P_2O_5	0.20	0.20	0.19	0.13	0.13	0.20	0.16	0.18	0.14	
LOI	7.40	11.6	11.0	11.5	12.1	13.4	16.2	12.7	12.4	
Total	100.76	101.52	101.06	101.85	101.68	102.20	102.95	101.89	102.03	
CIA	76.9	79.5	80.5	64.9	63.1	67.5	68.8	70.7	68.9	
Cwt%[a]	2.40	4.45	2.82	5.86	7.18	8.66	12.9	6.93	7.64	8.85
$\delta^{13}C$[b]	−29.6	−29.6	−28.3	−29.9	−30.0	−29.9	−30.1	−29.6	−30.1	−30.0

(*continued on next page*)

Table 1 (*continued*)

Sample	14EOS034	14EOS037	14EOS040	14EOS048	14EOS050	14EOS054	14EOS057	14EOS060	14EOS063	14EOS066
Stratigraphic height	1315	1324	1335	1343	1346	1349	1354	1359	1364	1369
Lithology	DMUU	DMUU	DMUU	ONW	ONW	ONW	ONW	ONW	ONW	ONW
Li	26.5	23.2	25.6	38.5	24.8	59.3	49.7	66.4	35.1	42.4
Be	2.63	1.67	1.19	3.31	2.05	5.00	4.47	4.67	2.86	3.36
Sc	7.39	10.2	9.52	20.0	13.5	27.9	27.4	30.1	18.2	21.8
Ti	0.27	0.29	0.26	0.43	0.29	0.55	0.58	0.67	0.38	0.43
V	176	237	214	910	593	1290	1180	1260	849	941
Cr	80.2	83.3	79.2	141	94.9	210	189	216	123	154
Co	6.30	7.64	8.20	46.5	7.07	14.8	16.3	34.6	18.2	78.9
Ni	56.6	44.9	57.9	140	26.0	55.9	32.7	106	96.4	115
Cu	23.4	16.0	26.4	9.06	4.41	4.33	29.3	8.80	26.5	6.30
Zn	684	111	201	130	1450	23.2	49.5	19.3	2870	33.8
Ga	11.3	13.2	12.5	21.0	14.6	29.9	28.6	30.2	19.8	22.7
As	0.30	1.96	80.8	82.3	6.85	16.4	14.4	28.6	12.4	102
Rb	73.0	73.4	68.5	165	107	252	244	261	166	195
Sr	156	155	181	51.1	182	80.4	97.1	78.2	87.1	79.1
Y	12.9	17.9	16.6	19.0	28.7	46.6	47.9	27.2	24.4	30.6
Zr	115	121	116	116	76.6	186	160	219	105	133
Nb	13.4	14.5	13.0	13.6	10.5	18.7	18.9	20.9	11.6	12.7
Mo	21.5	22.9	16.7	39.8	21.1	18.7	33.9	13.1	23.2	38.6
Ag	NA	NA	NA	NA	NA	NA	NA	NA	NA	NA
Cd	4.71	0.49	1.87	0.94	9.21	0.10	0.23	0.09	26.8	0.20
In	0.09	0.04	0.04	0.05	0.31	0.06	0.06	0.06	0.24	0.04
Sn	1.83	1.63	1.02	2.53	1.71	3.62	3.13	3.27	2.27	2.58
Sb	1.89	1.20	1.23	24.7	2.37	4.98	3.21	9.84	5.17	13.1
Cs	1.63	1.57	1.55	3.11	2.22	4.36	4.10	4.48	2.99	3.98
Ba	3280	2680	1890	3090	1360	2760	2220	2000	1320	1530
La	9.65	23.4	26.6	37.6	28.6	70.0	52.1	51.3	31.8	40.4
Ce	20.0	50.2	55.6	75.7	59.7	142	105	107	66.8	84.0
Pr	2.46	5.55	6.07	8.80	6.83	16.1	12.2	12.0	7.80	9.63
Nd	9.86	20.5	22.4	32.7	25.1	58.4	45.6	44.4	29.0	35.9
Sm	2.06	3.78	4.03	5.87	4.68	10.0	8.69	8.06	5.43	6.76
Eu	0.24	0.63	0.75	0.84	1.18	1.93	1.69	1.48	1.14	1.37
Gd	2.14	3.27	3.36	4.39	4.49	7.98	7.53	6.24	4.64	5.78
Tb	0.32	0.47	0.46	0.56	0.69	1.12	1.10	0.79	0.65	0.82
Dy	1.96	2.80	2.69	3.16	4.27	6.74	6.73	4.43	3.86	4.90
Ho	0.42	0.59	0.56	0.64	0.90	1.41	1.43	0.91	0.80	1.02
Er	1.24	1.70	1.59	1.87	2.60	4.04	4.09	2.67	2.26	2.89
Tm	0.19	0.25	0.23	0.29	0.39	0.62	0.62	0.44	0.35	0.45
Yb	1.27	1.60	1.50	2.02	2.59	4.12	4.09	3.23	2.32	2.97
Lu	0.19	0.24	0.23	0.33	0.41	0.65	0.65	0.58	0.38	0.48
Hf	2.85	3.00	2.89	3.01	1.97	4.76	4.20	5.65	2.75	3.52
Ta	0.77	0.86	0.76	0.95	0.70	1.22	1.34	1.45	0.83	0.88

W	4.16	1.82	2.57	4.20	2.55	5.17	5.85	6.04	8.62	4.00	
Tl	1.08	1.05	1.03	2.34	1.57	3.36	3.22	3.20	2.40	2.90	
Pb	64.9	7.69	5.74	18.0	7.24	15.9	8.82	24.0	19.5	27.0	
Th	6.20	7.24	6.73	10.3	7.15	15.9	14.6	16.8	9.02	11.8	
U	7.99	8.86	8.16	16.4	13.3	17.4	19.9	22.3	12.4	16.6	
Nb/Ta	17.55	16.91	17.14	14.33	14.99	15.24	14.07	14.39	13.95	14.52	
Zr/Hf	40.44	40.21	40.35	38.56	38.90	39.06	38.15	38.79	37.97	37.84	
Nb/Th	2.167	2.005	1.929	1.317	1.470	1.173	1.290	1.244	1.288	1.078	
Y/Ho	30.57	30.30	29.83	29.50	31.79	32.92	33.59	29.82	30.39	30.00	
U/Th	1.289	1.224	1.212	1.596	1.861	1.095	1.362	1.329	1.376	1.406	

[a] Samples yielding too little hand-picked matrix could not be analysed for major elements.
[b] Cwt%: Mass fraction of C per total sample mass. Calculated as $Cwt\% = (M_C/M_{total}) \times 100\%$ where M is the mass (g).
[c] $\delta^{13}C$: Calculated as $[(({}^{13}C/{}^{12}C)_{sample}/({}^{13}C/{}^{12}C)_{standard}) - 1] \times 1000‰$.
[d] NQ: In two analytical runs, no successful detector cross-calibration was achieved for Ti, V, Rb, Ba and Ce. In these cases analogue signals were not quantified (NQ).
[e] BDL: Two analytical runs were affected by poor Zn blanks. Signals smaller than 3 × blank were considered below detection limit (BDL).
[f] NA: In one analytical run, the internal standard contained Ag, therefore Ag was not analysed (NA).

subtle but significant difference in HFSE variability exists between the Sandcherry Member and the Dowling Member. This discrepancy is most noticeable in the relative abundances of the elements Nb, Ta, Zr and Hf. Fractionation between these elements is widely attributed to magmatic source processes. The Nb/Ta ratios range between 13.7 and 18.3 in the Sandcherry member with an average of 15.1 ± 1.3, while in the Dowling Member the ratio ranges from 14.6 to 18.5 with an average of 15.9 ± 0.7. The Zr/Hf ratios in the Sandcherry Member range from 38.8 to 40.3 with an average of 39.8 ± 0.5, while in the Dowling Member the ratios range from 38.7 to 41.5 with an average of 40.0 ± 0.6 (Table 1). There is a positive correlation between Nb/Ta and Zr/Hf ($r^2 = 0.623$, Supplemental Fig. 3A), both ratios increasing up section, particularly in the middle and upper units of the Dowling Member (Fig. 3). In strong contrast, the Onwatin Formation displays significantly lower ratios, Nb/Ta ranging from 14.0 to 15.2, and Zr/Hf ratio ranging from 37.8 to 39.1, with averages of 14.5 ± 0.5 and 38.6 ± 0.5, respectively.

The relative abundances of the rare earth elements (REEs) and extended trace elements are likely an indication of the relationship between the Onaping Formation ash matrix and associated facies, and may aid the reconstruction of the origin of the ash. Rare earth elements and extended trace elements are plotted normalised to the vitric rim of the Trill offset dyke composition (sample 12-JAP-022, this study) in Fig. 4, for comparison with the original shock impact melt. The REE pattern normalised to the SIC (modified from Lightfoot et al., 1997) and the extended trace element pattern normalised to upper continental crust (UCC, McLennan, 2001) are displayed in Supplemental Fig. 4A and B, respectively. All units of the Onaping Formation show strong similarity with the offset dyke and the SIC, yielding flat patterns with values close to 1. Both the Sandcherry Member and the Dowling Member units show a negative Eu anomaly compared to the putative impact melt, possibly an effect of plagioclase fractionation during crystallisation.

4.2.2. Volatile elements

Chemical stratigraphies of the metals Pb and Sb are displayed in Fig. 5. A large apparent depletion exists in both elements in the Sandcherry Member and the Contact Unit of the Dowling Member. Concentrations become more widely varied from the Lower Unit of the Dowling Member upwards. Concentrations of Pb range from 0.34 ppm to 6.09 ppm in the Sandcherry Member with an average of 1.63 ± 1.70 ppm. The concentration in the Dowling Member ranges between 0.78 ppm and 17.5 ppm with an average of 5.13 ± 3.17 ppm. Supplemental Fig. 3B shows the deficiency in Pb compared to UCC. In a similar manner, concentrations of Sb in the Sandcherry Member range from 0.05 ppm to 0.19 ppm with an average of 0.11 ± 0.04 ppm, rising to a maximum of 1.20 ppm in the Dowling Member. Pb concentrations in the Onwatin Formation range from 7.24 ppm to 27.0 ppm, while Sb concentrations range from 2.37 ppm to 24.7 ppm. It is noted that both these elements are moderately volatile. Similar but more complex trends exist for many more metals, however this

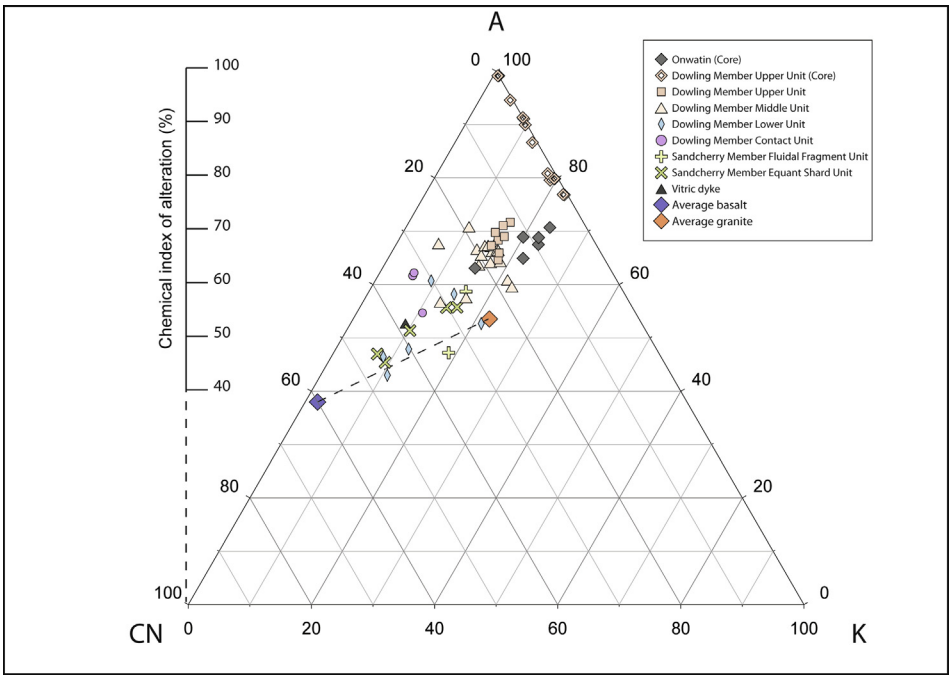

Fig. 2. Al_2O–$(CaO^* + Na_2O)$–K_2O (A–CN–K) ternary plot showing the degrees of alteration experienced by the different units of the Sandcherry Member, Dowling Member and Onwatin Formation (Nesbitt and Young, 1982). The chemical index of alteration (CIA, Fedo et al., 1995) is shown on the left, relative to the A–CN–K plot. The Trill offset dyke, average basalt and average granite are shown for comparison.

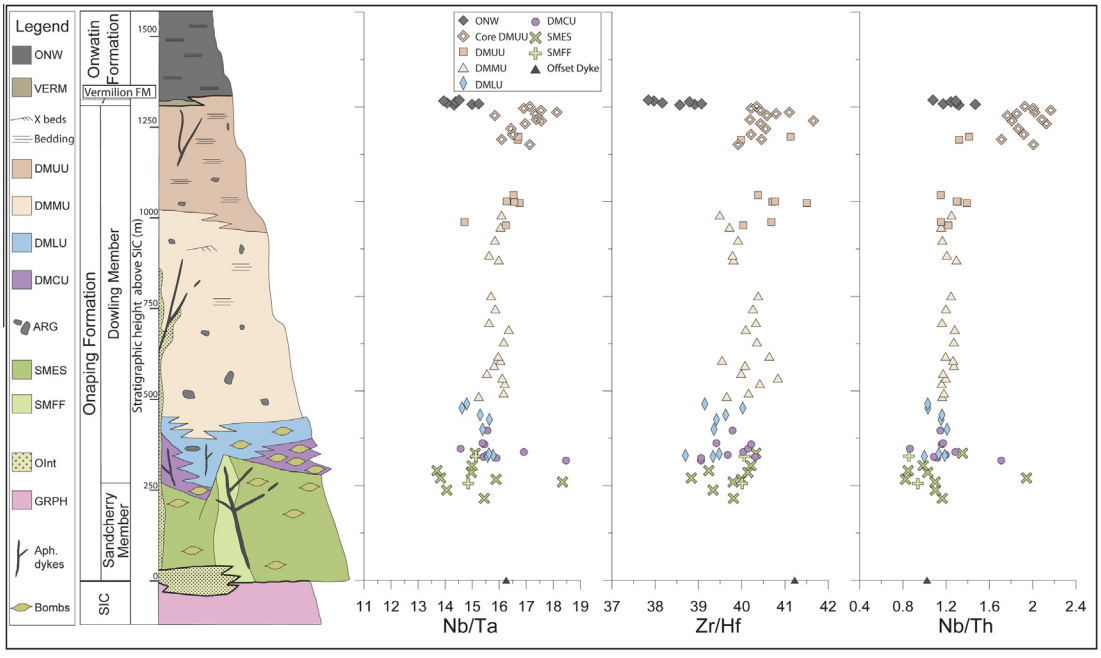

Fig. 3. Stratigraphic column of the Onaping and Onwatin Formations with selected trace element chemostratigraphies Nb/Ta, Zr/Hf and Nb/Th. Abbreviations: ONW, Onwatin; VERM, Vermilion; DM, Dowling Member; UU, Upper Unit; MU, Middle Unit; LU, Lower Unit; CU, Contact Unit; SM, Sandcherry Member; FF, Fluidal Fragment Unit; ES, Equant Shard Unit; OInt, Onaping Intrusion; GRPH, Granophyre; ARG, argillite clasts.

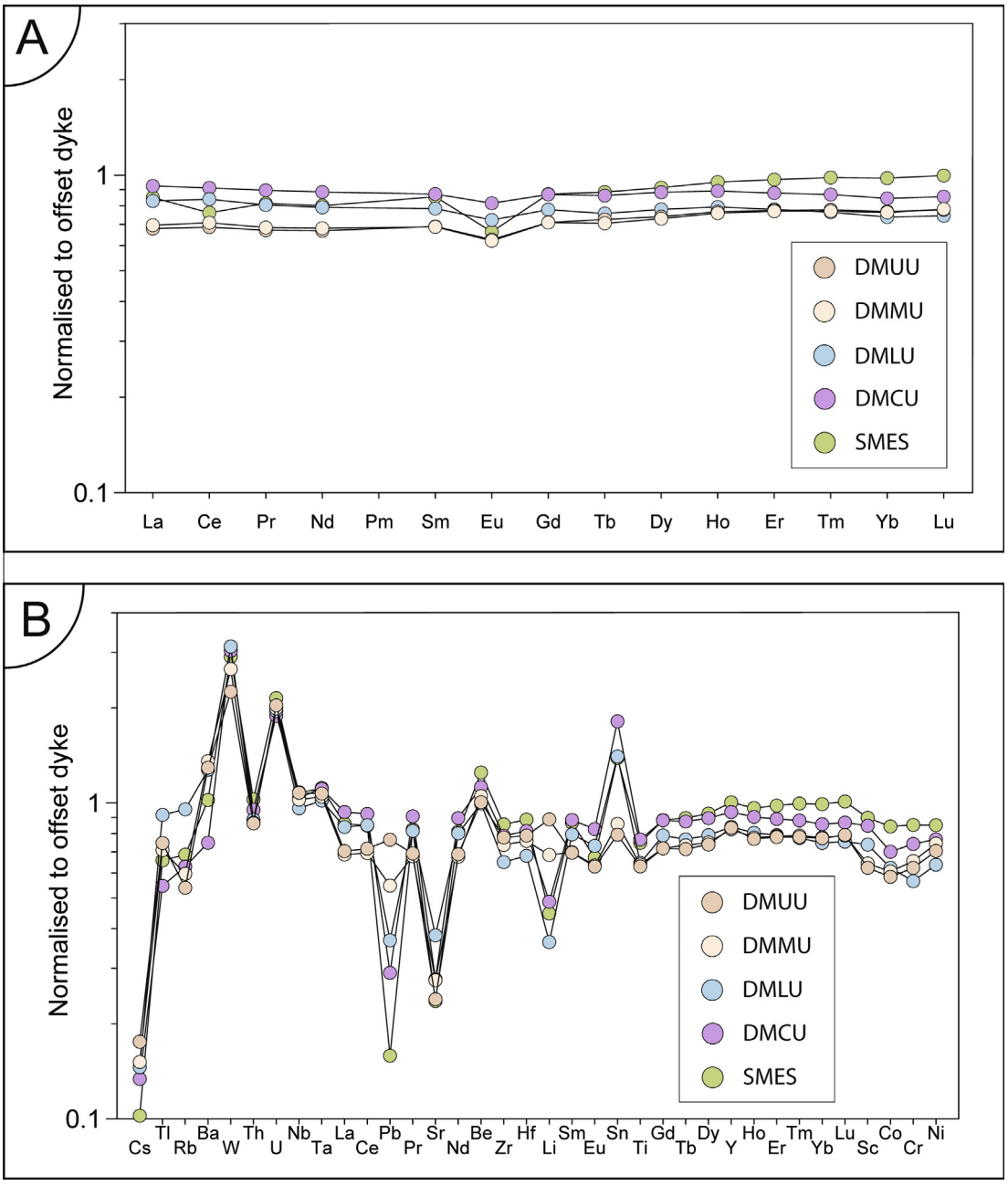

Fig. 4. (A) Trill offset dyke-normalised REE plot for the Sandcherry Member and individual units of the Dowling Member; (B) Trill offset dyke-normalised extended trace element plot for the Sandcherry Member and individual units of the Dowling Member.

analysis is beyond the scope of this paper and will be the subject of a subsequent, more detailed study.

4.2.3. Seawater sensitive elements

Several of the analysed elements are well known for their affinity for seawater and saline groundwater (e.g., Byrne and Lee, 1993; Bau and Dulski, 1999). By way of example, Y and U are presented as chemostratigraphies of the ratios Y/Ho and U/Th because of the known subaqueous emplacement of the Onaping Formation (Fig. 5). The Y/Ho curve shows significant Y enrichment in the entire Onaping Formation with respect to the vitric rim of the Trill offset dyke, increasing from a minimum Y/Ho ratio of 26.0 in the Sandcherry Member to a maximum of 29.2 in the upper Dowling Member. This is mirrored in the U/Th ratio, which increases from 0.35 at the base to 0.66 at the top of the Onaping Formation. The offset dyke displays a typical crustal Y/Ho ratio of 25.8 and U/Th ratio of 0.22.

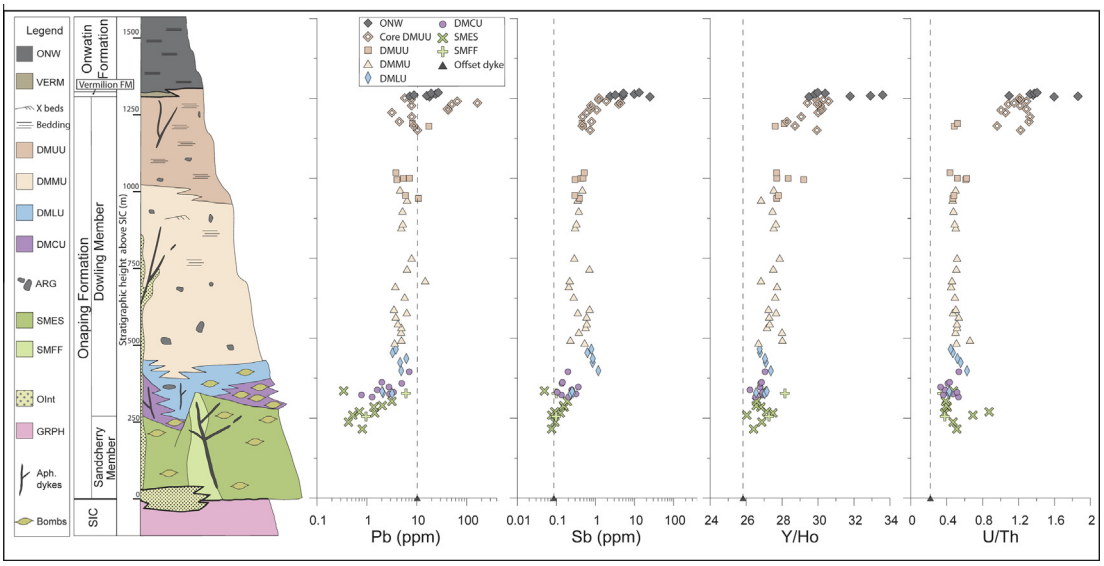

Fig. 5. Stratigraphic column of the Onaping Formation and Onwatin Formation showing concentrations of volatile elements Pb (ppm) and Sb (ppm) and seawater sensitive ratios Y/Ho and U/Th. Abbreviations as in Fig. 3.

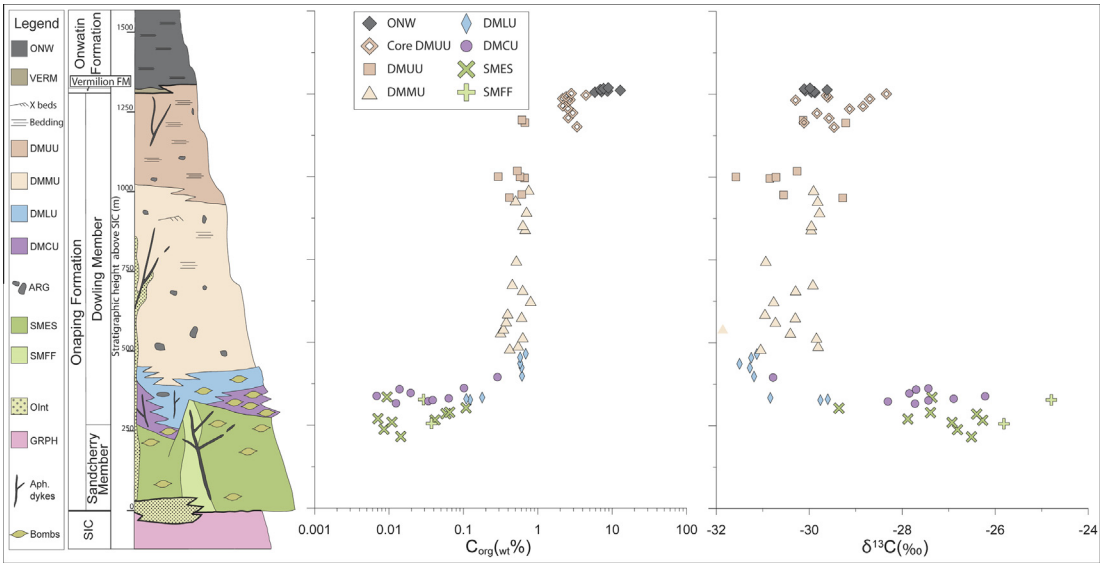

Fig. 6. Stratigraphic column displaying increase in $wt\%_{org}C$ and C-isotopes for all samples of the Onaping Formation and Onwatin Formation. Abbreviations as in Fig. 3.

Y/Ho and U/Th ratios both increase significantly across the boundary to the Onwatin Formation to a maximum of 33.6 and 1.86, respectively.

4.2.4. Cwt% and C-isotopes

Fig. 6 displays the results obtained by IRMS analysis. In terms of stratigraphy, carbon content (wt%C) increases from negligible amounts in the Sandcherry Member through the Dowling Member to significant concentration in the Upper Unit and the Onwatin Formation, to a maximum of ~13 wt%. Carbon isotope ratios reveal a sudden and significant decrease in $\delta^{13}C_{org}$ in the Contact Unit of the Dowling Member to values ca. −31‰. This value remains constant throughout the remainder of the basin fill.

4.2.5. Redox-sensitive elements

Several further metals show a behaviour typical of marine sediments (e.g., Algeo and Lyons, 2006; Xu et al., 2012; Asael et al., 2013). Fig. 7 shows chemostratigraphies of redox sensitive elements Mo and V. Vanadium decreases in concentration up stratigraphy of the Onaping Formation, from a maximum of 187 ppm in the Sandcherry Member to a minimum of 69.3 ppm in the Upper Unit of the Dowling Member. This gradual decrease in concentration

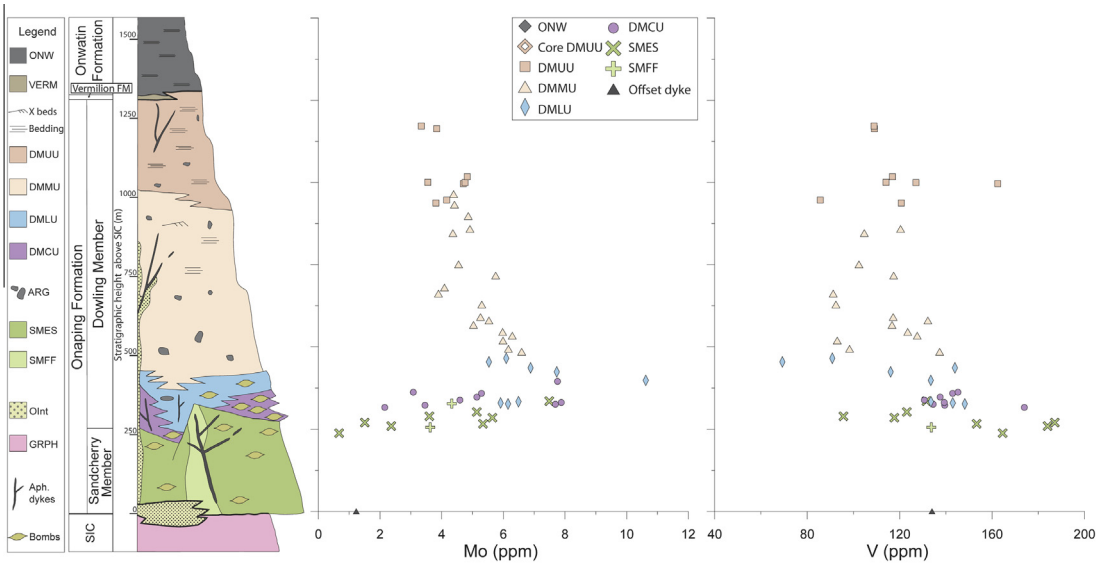

Fig. 7. Stratigraphic column showing concentration of Mo and V in Onaping Formation. Concentrations are shown in ppm. Abbreviations as in Fig. 3.

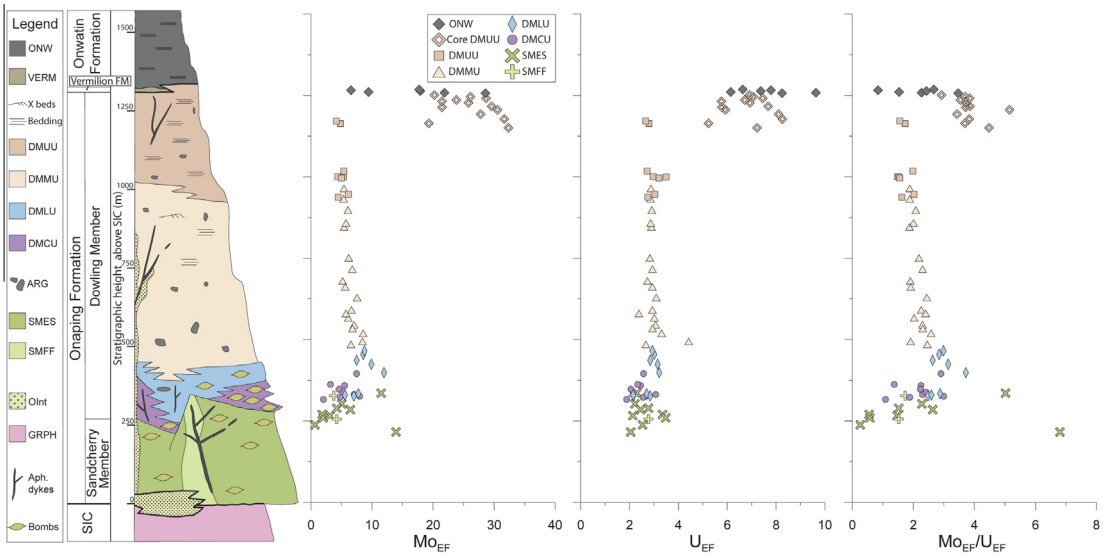

Fig. 8. Stratigraphic column showing enrichment factors (EFs) of Mo and U, calculated as $X_{EF} = [(X/Al)_{sample}/(X/Al)_{PAAS}]$, where X and Al stand for the weight concentration of elements X and Al, respectively (EF, Algeo and Tribovillard, 2009). The third column shows a comparison of MoEF and UEF up stratigraphy. Abbreviations as in Fig. 3.

can also be seen in elements such as Cr and Co (Table 1). In contrast, Mo is depleted in the Sandcherry Member, with a minimum of 0.67 ppm followed by a sharp surge in concentration to a maximum of 17.5 ppm near the contact unit of the Dowling Member. This trend is reversed by a gradual decrease in the Dowling Member to a minimum of 3.34 ppm at the top. A second surge in Mo concentrations is then shown by samples collected from the core, increasing suddenly through the boundary between the Onaping and Onwatin Formations (e.g., Fig. 8), to a maximum of 39.8 ppm in the Onwatin Formation.

4.2.6. Argillites

Three samples of argillite clasts were analysed only for trace elements. The clasts display low Nb/Ta and Zr/Hf ratios closer to that of the Onwatin Formation and the UCC. Rare earth element patterns also show a closer relationship to the Onwatin Formation. The Y/Ho ratios are similar to those of the Dowling Member and lower than that of the Onwatin Formation. Molybdenum concentrations are slightly lower than in the Dowling Member and much lower than in the Onwatin Formation.

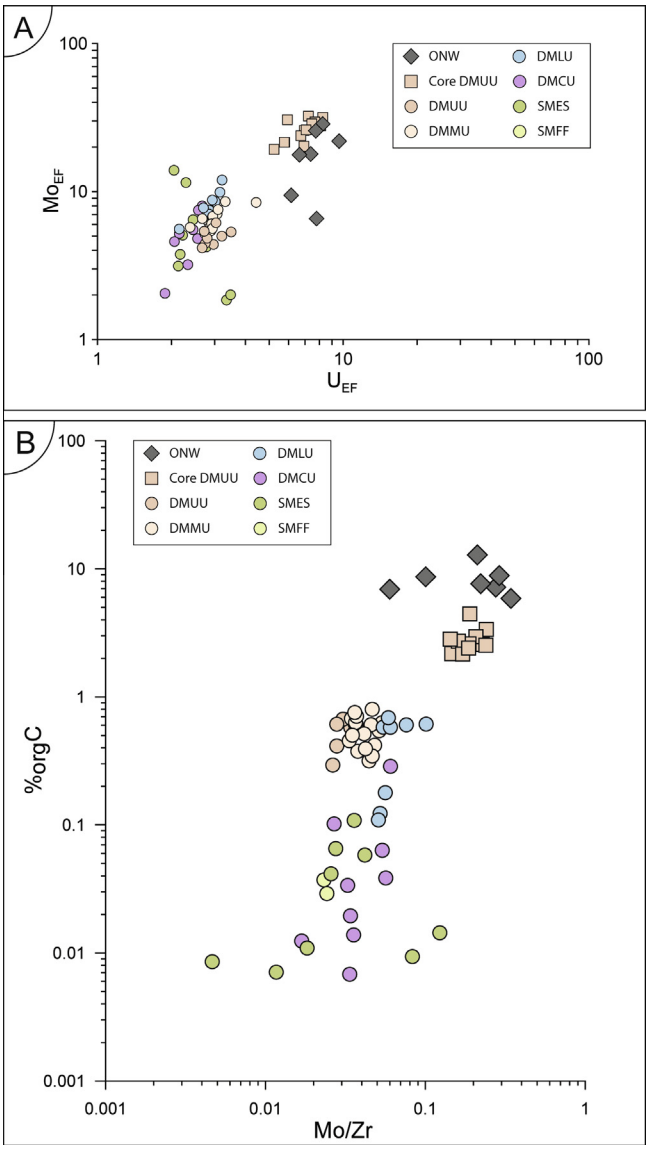

Fig. 9. (A) Bivariate plot of enrichment factors of Mo and U (MoEF and UEF, respectively) for comparison with plots after Algeo and Tribovillard (2009). EF calculated as in Fig. 8. (B) Bivariate plot comparing amount of organic C and concentration of Mo in the Onaping Formation. Abbreviations as in Fig. 3.

5. DISCUSSION

The results obtained in this study represent the first comprehensive geochemical database from which a detailed reconstruction of a large impact crater fill evolution can be inferred. The discussion will focus on three aspects of this reconstruction: the impact-related features of the fill; the stratigraphic evolution of the ash matrix source; and the interaction of the rocks with the basin water.

5.1. Impact-related features

Ahead of this discussion it is worth stressing that the data presented in this study were obtained by analysis of carefully hand-picked granules of ash-sized (<2 mm) particles that constitute the breccia and tuff matrix, in order to minimise the complexities associated with lithic target rocks and post-impact magmatic products, allowing the best possible comparison of the Onaping Formation with pristine impact melt proxies and UCC. For the purposes of clarity, only samples collected from Joe Lake will be discussed initially, with reference to samples recovered from the drill core later in the section.

5.1.1. Comparison with impact melt

Unlike ordinary terrestrial melts, the unusual origin of impact melts coupled with their complex emplacement and post-impact history does not permit comparison of the full suite of major and trace elements that were analysed. For reasons that will become apparent in the following sections of the discussion, the initial comparison is here

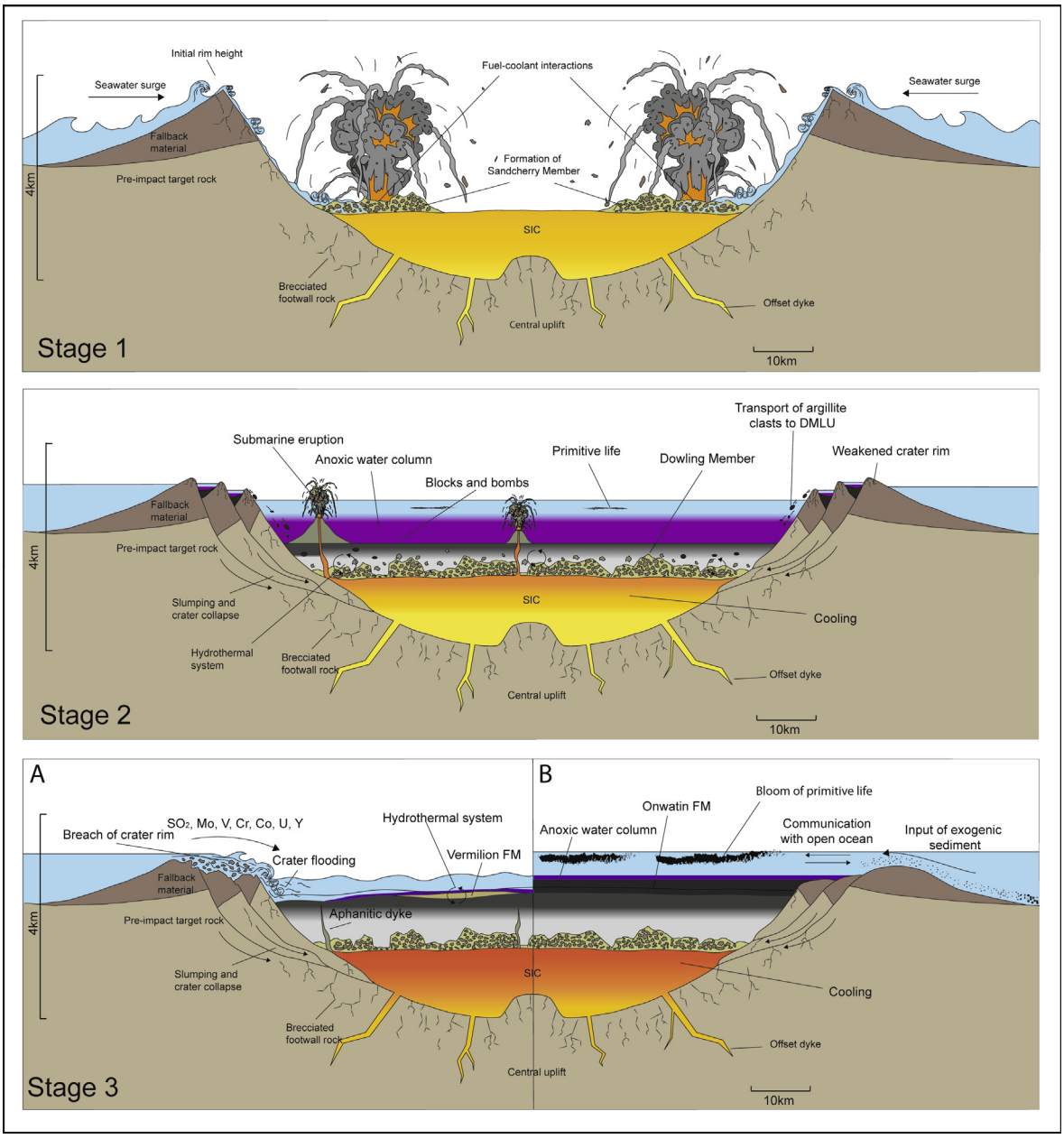

Fig. 10. Stage 1: Slumping of initial crater rim created a multi-rim structure containing an impact melt pool. Backwash of tsunami-like waves triggered by the impact washed over the sides of the crater, interacting explosively with the melt sheet. Fragmented melt cooled and solidified to form the Sandcherry Member. Stage 2: The Sandcherry Member covered the cooling melt sheet, as vents continued to feed melt to the surface of the fill. Water filled the crater during a catastrophic collapse of the Sandcherry Member and lower Dowling Member, with which the melt continued to interact, forming the contact and lower units of the Dowling Member. Activity diminished over time, leading to a decrease in vitric shard size up section. Argillitic muds were deposited in the outer reaches of the structure, and transported by debris flows to the lower Dowling Member as the crater rim began to erode. Life began to colonise the surface waters, eventually causing anoxia in the deeper water column. Organic matter settled through the water column, scavenging many particle-reactive elements including Mo, V, Cr, and Co, causing a reservoir effect. Stage 3: (A) Continued volcanism constructed the Middle and Upper Dowling Member. The final breach of the crater rim at the NE and SW apices allowed seawater to surge over the rim, replenishing the water column with transition metals and sulphate. Hydrothermal deposition was temporarily re-established, forming the Vermilion Formation VMS deposits. (B) Volcanism eventually ceased, and communication with the open ocean allowed the transport of sediment into the basin, constructing the Onwatin Formation.

conducted using only alteration resistant major elements, the REE and selected HFSEs.

Although the vast SIC and the voluminous Onaping Formation essentially derived from the shattering and shock melting of granites, gneisses, metasediments and metavolcanics of the Southern Province, Huronian Supergroup and the southernmost Superior Province (Therriault et al., 2002), previous analyses of Pb-isotopes

and trace element data suggest that at no point was the impact melt fully chemically homogenised (Darling et al., 2010a,b). In addition to incomplete homogenisation, the insulated melt sheet must have continued to thermally erode and assimilate footwall rock (e.g., Darling et al., 2010b), thereby modifying the bulk composition of the SIC. Furthermore, the melt sheet subsequently differentiated into three chemically distinct layers as it cooled (Naldrett et al., 1970; Therriault et al., 2002).

This continuous chemical evolution of the SIC complicates an accurate estimate of the impact melt via the SIC and comparison with other impact melt proxies, such as the Onaping Formation matrix. Nonetheless, in terms of major elements, the ash matrix appears largely similar to the average SIC calculated by Lightfoot (1997), Lightfoot and Doherty (2001) and Therriault et al. (2002). SiO_2 values of the Sandcherry Member and the Dowling Member are almost identical ($62.6 \pm 3.0\%$ and $62.5 \pm 1.4\%$, respectively), slightly higher than the average SIC (64.2%, Lightfoot, 1997), and resemble typical upper continental crust (UCC) values (Taylor and McLennan, 1985). With respect to Al_2O_3, the Sandcherry Member ($12.6 \pm 0.9\%$) and the Dowling Member ($11.0 \pm 0.9\%$) are close to the average SIC value of 13.83%. In contrast, there is a slight deficit in the TiO_2 in the Sandcherry Member ($0.59 \pm 0.10\%$) and the Dowling Member ($0.45 \pm 0.05\%$) compared to the average SIC of 0.78% (Lightfoot, 1997). This is not a method bias in our data as the Ti measurements between the separately prepared major (ICP-OES) and trace element (ICP-MS) analyses agree to within 4% ($r^2 = 0.929$). Another complication to this comparison stems from the possible alteration of the Onaping ash matrix as a result of post impact interaction with hydrothermal fluids and seawater (Ames et al., 1998, 2006). However, the observed CIA values of the carefully hand-picked samples selected to avoid visible alteration (such as albitization) at Joe Lake indicate a variable extent of alteration, mostly between ~45 and ~70 (Fig. 2). None of the samples collected from the field show extensive alteration that could be attributed to sub-recent weathering. The extent of alteration appears to increase with increasing stratigraphic height. It is possible that this increase could represent the gradual introduction of mud particles to the crater, as discussed in Section 5.2.3, rather than alteration of the ash particles. The Onwatin Formation mudstones show a different style of alteration, having experienced K-addition typical of mudrocks (e.g. Fedo et al., 1995). The limited alteration of Onaping Formation matrix is also evident from the fact that Al_2O_3 values of the Sandcherry Member ash matrix fall within the range of both the SIC and the offset dyke. Namely, higher Al_2O_3 indicating alteration of volcanic rocks by conversion of primary phases and glass to sheet silicates (e.g., Babechuk et al., 2014), is not observed.

A striking feature of the new dataset with respect to the REE and the HFSE is the limited variability throughout the chemostratigraphy, demonstrated most clearly with the average Nb/Ta, Zr/Hf and Nb/Th ratios that remain largely constant throughout the stratigraphy (Fig. 3). Therefore, in many aspects, the chemistry of the ash matrix has remained nearly uniform across ca. 1.4 km of stratigraphy. This testifies to the successful isolation of ash matrix by careful hand-picking. The homogeneity also demonstrates the need for high precision data to appreciate the significance of finer scale variability. In terms of overall composition, it has long been shown (e.g., Darling et al., 2010a) that the impact melt at Sudbury strongly resembles UCC. This similarity is confirmed by the UCC-normalised REE patterns of the Onaping Formation ash matrix, in contrast to the lower crustal composition suggested by Mungall et al. (2004). Supplemental Fig. 4C shows the average SIC-normalised REE patterns for the Sandcherry ($n = 11$) and Dowling Members samples ($n = 43$). They are identical within 1σ standard deviation and have a very flat horizontal pattern deviating only marginally from 1.

In terms of comparing the ash matrix with putative impact melt, the most pristine samples of the original shock melt possibly come from inclusion-free vitric rims of dykes that radiated from the original impact melt sheet (Lightfoot et al., 1997). A single sample of this quenched melt from the Trill offset dyke was analysed in duplicate in this study and used to normalise Onaping Formation ash matrix REEs. The resulting pattern, shown in Fig. 4A, shows beyond reasonable doubt that the bulk of the ash matrix is indistinguishable from the Trill offset dyke vitric margin. In terms of HFSE, one sample aliquot of the Trill offset dyke was prepared using a WC mill and cannot be used to evaluate the HFSE. However, the agate mortar-prepared sample has HFSE systematics that compare very well with average Onaping Formation matrix. The Nb/Ta ratio of the offset dyke is 16.3, similar to the average Dowling Member ash matrix (15.9 ± 0.7) and within error of the Sandcherry Member average (15.1 ± 1.3). In a similar manner, the Zr/Hf ratio of the offset dyke (41.2) compares well with the Sandcherry Member (39.8 ± 0.5) and even more so with the Dowling Member (40.0 ± 0.6). The Nb/Th ratio also shows correspondence between the offset dyke (1.02) and the Sandcherry Member (1.10 ± 0.32), but the Dowling Member is somewhat depleted in Th relative to the offset dyke (1.20 ± 0.13). The close correlation in these trace elements clearly indicates a close relationship between the sources of both sample types.

Whereas the offset dyke margins can be regarded as the most pristine remnants of the shock melt, it is also possible that they experienced modification from wall-rock interaction or they could represent a more local impact melt that was never fully homogenised (Darling et al., 2010b). By contrast, the volumetrically most important proxy for impact melt is the putative differentiated impact melt sheet, the SIC. The most widely used average composition for the SIC was published by Lightfoot et al. (1997). However, as with many compilations, this average was calculated by combining data from several sources obtained by many different analytical techniques, resulting in varying degrees of accuracy, particularly for the mono-isotopic REE. These inconsistencies become obvious when the REE pattern of the average SIC compiled by Lightfoot et al. (1997) is normalised to UCC, revealing several irregular spikes in the elements Pr, Tb, Dy and Lu. So as not to introduce artefacts into SIC-normalised REE patterns, the compiled

values for these elements were modified (where Pr = 10.6; Tb = 0.88; Dy = 4.95; Lu = 0.375) to yield a smooth UCC-normalised pattern for the SIC average. When normalised to this new SIC composite (Supplemental Fig. 4C), the Sandcherry Member and Dowling Member averages again plot as horizontal flat patterns. They are less enriched in Eu, which may be related to fractionation of plagioclase within the SIC.

Notwithstanding the similarity of the Onaping Formation ash composition with vitric offset dyke and average SIC (and the UCC), the small and significant discrepancies reveal additional insight. This variability mainly concerns the larger heterogeneities evident in the Sandcherry Member versus the Dowling Member, the contrast most notably shown by the Nb/Ta and Zr/Hf ratios (Fig. 3). In the Sandcherry Member, the RSD in Nb/Ta is 8%, whereas that of the Dowling Member is only 4%, and furthermore the RSD for the most chemically homogenous section of the fill (middle and upper Dowling Member) is even smaller at 3%. The greater chemical variability in the Sandcherry Member could have two main possible explanations. Firstly, it could reflect true unhomogenised variability of locally melted target rocks that make up the matrix of the lower fill. In the field, component analysis conducted by grid surveys revealed that the Sandcherry Member and the lowermost Dowling Member contain the largest volume and variability of partially assimilated lithic fragments. The Sandcherry Member also contains a much greater variability in U/Pb zircon ages than the Dowling Member (Petrus et al., 2015b). The survival of partially-melted lithic fragments could indicate that local melt heterogeneity persisted in the lower crater fill. The second possibility is that the greater chemical variability could be an artefact of incomplete separation of fragmented lithic clasts during preparation in the laboratory. Matrix is much less abundant in the Sandcherry Member and for this reason much more difficult to hand-pick. The majority of samples in this study were diligently hand-picked at Trinity College, Dublin over the course of four months. However, one batch of samples had been separated in an earlier study (Petrus et al., 2015a) with less attention to detail. Inspection of the two datasets reveals that they show nearly identical degrees of heterogeneity. For example, in terms of Nb/Ta, they yield RSDs of 6.8% (carefully hand-picked samples) and 6.7% (rapidly picked, larger samples), respectively. The observation that the variability persists regardless of the effort put into the preparation of the samples leads to the conclusion that the observed heterogeneity in the Sandcherry Member is likely derived from variable degrees of assimilation of fragments that may have varied locally in the target rocks. Furthermore, this change occurs after a distinct period of crater reorganisation (Ames et al., 2002) and precedes a period of volcanism within the crater (Ames et al., 2002). The variability diminishes up section and will be analysed in more detail later in this discussion.

In summary, in terms of least mobile major elements, REE and HFSE, the ash-sized matrix of the entire Onaping Formation is very homogenous and resembles closely the composition of the entire SIC and a well-preserved vitric offset dyke. The chemical variability is greater in the lower portion of the stratigraphy, namely the Sandcherry Member and the lower Dowling Member. This is attributed to incomplete impact melt homogenisation. Overall, the ash-sized matrix shares many attributes with average UCC.

5.1.2. Volatile element loss

In view of the very limited variability in refractory trace element content in the ash-sized matrix of the entire Onaping Formation, and considering the close match in chemistry with other proxies of the impact melt, it could be expected that these similarities would extend to other elements also. However, unlike standard terrestrial melts, which form at depth and are later emplaced higher in the lithospheric column, impact melts form very differently. The catastrophic release of enormous energies in very large impacts (several 10^8 MegaTons TNT for a crater between 150 and 200 km in diameter), leads to near-instantaneous melting and vaporisation in a plasma. Other effects include very high thermal radiation (e.g., thermal exposure of $>10^{10}$ J/m^2) and an air blast with modelled peak wind velocities of >2000 m/s (Collins et al., 2005). Under such conditions, volatile elements are expected to be vaporised and lost from the impact site. Although volatile element loss has been inferred to explain the Earth's general depletion in Pb and other elements (e.g., Allegre, 1968) and has also been speculated to contribute to the high U/Pb ratio of lunar impact glass (Nemchin et al., 2011), no systematic study of volatile elements in a large impact structure has yet been published. Our study presents a wide set of trace element data, including volatile elements in the Onaping Formation. In this section, we will limit the discussion to the moderately volatile elements Pb and Sb. A full analysis of all volatile elements will be the focus of a separate study.

By contrast to the monotonous chemical stratigraphies for refractory elements (e.g., Fig. 3), the chemostratigraphies of Pb and Sb show very pronounced topography. Fig. 5 demonstrates the very severe depletion in the Sandcherry and lower Dowling Members. The Sandcherry Member Pb concentrations range from as low as 0.34 ppm to a maximum of 6.09 ppm (Table 1), deviating from the expected UCC value of 20 ppm (McLennan, 2001) by a factor of up to ~50. This extreme apparent depletion is consistent through the full suite of Sandcherry Member and lower Dowling Member samples. Secondly, the depletion is followed by a sharp and consistent increase in Pb concentrations up-stratigraphy in the middle and upper Dowling Member, where concentrations shift towards more typical UCC values to a maximum of 17.5 ppm (Table 1), indicating a transition to sourcing material from a source that did not experience Pb depletion. This systematic trend is mimicked by concentrations of Sb (Fig. 5), ranging from 0.05 ppm to 0.19 ppm in the Sandcherry Member, generally depleted relative to UCC (0.2 ppm, Taylor and McLennan, 1985). Other transition metals, including the redox-sensitive Mo, show similar but more complicated trends that will be discussed in Section 5.3.3.

Three possible explanations for the distinctive chemostratigraphies of Pb and Sb are discussed. Firstly, it appears possible that the separation of an immiscible sulphide melt from the silicate melt sheet exhausted available

Pb and that Sandcherry Member matrix was sourced from the silicate. Lightfoot and Doherty (2001) reported sulphide ores within the offset dykes with elevated Ni, Cu and PGEs that are thought to have crystallised from an original Ni- and Cu-rich melt that later became depleted in these elements. However, this is generally considered to have happened only upon cooling of the melt sheet. Furthermore, the Sandcherry Member clasts are typically melt-coated and believed to have been emplaced immediately after the impact (Grieve et al., 2010; Supplemental Fig. 2B). Regardless, the critical observation regarding the sulphide melt is that it was apparently very poor in Pb, resulting in unusually radiogenic Pb-isotope compositions of SIC-hosted sulphide (Darling et al., 2010a,b). We also note that more recent experimental studies have questioned whether Pb is as chalcophile as was previously assumed (Lagos et al., 2008). It is therefore considered unlikely that the observed depletion in Pb in the Sandcherry Member could have been caused by Pb-sequestration into a very early sulphide melt.

Secondly, there is the possibility that Pb concentrations were initially high, similar to average UCC, but subsequent pervasive hydrothermal alteration could have removed Pb and Sb. Alteration of the components of the Onaping Formation have previously been attributed to an active hydrothermal system, and several types of alteration at Joe Lake have been identified and mapped in detail (Ames et al., 1998; Ames and Gibson, 2004). If alteration was stronger in the Sandcherry Member samples analysed in this study, this could have led to the mobilisation of Pb (and Sb) and resulted in the apparent depletion evident in the chemostratigraphy. However, the observed CIA values in the Sandcherry Member and lower Dowling Member (~45–60) are consistently lower than the middle and upper Dowling Member (~60–70), implying that they experienced less alteration. Furthermore, there is no correlation between extent of Pb depletion, as estimated from Pb/Nd (e.g., Miller et al., 1994; Kamber et al., 2002) versus the CIA (Supplemental Fig. 3C).

The remaining explanation, in light of the extreme conditions experienced by the target material upon impact, is that at least some of the more volatile elements that are concentrated in crustal rocks were lost during impact vaporisation (e.g., Sharp and Draper, 2013). This process, caused by highly energetic collisions between large masses during late stage planetary accretion, has been previously proposed as a mechanism of the preferential loss of incompatible elements from the surface environments of early forming planetary bodies (O'Neill and Palme, 2008). Sharp and Draper (2013) suggested that 'impact erosion' during recurrent large to giant impact events depleted the crust in the highly volatile halogens Cl and Br. Here we propose that by analogy to the halogens, loss of at least some of the metallic elements with low boiling points could occur during impact erosion.

The depletion in Pb and Sb in the Onaping Formation, among many other moderately volatile elements, ends at a distinct transition marked by growth faulting and collapse during a stage of impact crater modification, followed by the initiation of volcanism within the crater (Ames et al., 2000, 2002). As such, the volatilisation of the lower fill is part of a complex geochemical evolution. This volatile loss will require further comprehensive research, guided by experimental insight (e.g., Ebert et al., 2014).

5.2. Evolution of matrix source

Several simultaneously operating processes are required to explain the petrology of the progression from the lithic clast-dominated Sandcherry Member to the glass shard- and ash-dominated lower Dowling Member. The homogenous chemostratigraphies observed in the ash matrix as described earlier and the apparent chemical similarity between the ash matrix and impact melt at first do not appear to reflect this change. Accordingly, more subtle variation in the geochemistry were investigated.

5.2.1. Impact melt source and change in lithophile element ratios

A previous investigation of the chemical composition of the impact melt (Mungall et al., 2004) primarily focused on the PGEs and selected transition metals of the Onaping Formation matrix and the offset dykes. Their results provided reasonable evidence to support the crustal origin of the melt sheet and offset dyke, and argued against a contribution from a mantle source. However, transition metal concentrations of the impact melts were found to be too high to be sourced from typical UCC alone. This observation was argued to require a contribution from the lower crust, although we note that the composition of the local lower crust is unknown. Working with a larger dataset, Petrus et al. (2015a) postulated that the PGE content and patterns in the Onaping Formation also required a contribution from a previously unrecognised Mg-rich mafic target rock.

The contribution from a mafic source to the SIC and the Onaping Formation matrix is also required because of the Nb/Ta and Zr/Hf ratios reported here. In terms of Nb/Ta and Zr/Hf, the Onaping Formation, offset dyke and SIC do not match the UCC. The Dowling Member Nb/Ta ratio (15.9 ± 0.7) is much too high to be sourced from typical UCC alone (~11.0–13.0, Taylor and McLennan, 1985; Green, 1995; Rudnick and Fountain, 1995; Barth et al., 2000), and suggests a significant contribution from a more mafic source to produce the observed impact melt composition with a Nb/Ta ratio more typical of the mantle (15.0–16.0, Pfänder et al., 2007), mid ocean ridge basalt (MORB) (~13.0–16.0, Münker et al., 2003; Workman and Hart, 2005; Arevalo and McDonough, 2010) or ocean island basalt (OIB, ~14.5–17.5, Green, 1995; David et al., 2000; Pfänder et al., 2007). The observed high mafic Nb/Ta signatures are supported by the elevated Zr/Hf ratios relative to the UCC (36.0–38.0, David et al., 2000). The average Zr/Hf ratio of the Dowling Member is 40.0 ± 0.6, suggesting the source of the ash matrix was more similar to OIB composition (39.0–43.0, David et al., 2000) or MORB (41.0, Arevalo and McDonough, 2010). Although melting of the lower continental crust may have contributed to the impact melt as speculated by Mungall et al. (2004), these ratios are not representative of typical lower continental crustal concentrations (McLennan, 2001). Furthermore, it is unlikely

that the local UCC that was impacted had unusually high Nb/Ta and Zr/Hf ratios because LaFrance and Kamber (2010) reported Nb/Ta and Th/U ratios of Southern Province rocks much lower than the values found here. Despite the heterogeneity of the Sandcherry Member, which likely arose from the variable compositions of target rock lithologies, the unusual enrichments in Nb and Zr (relative to Ta and Hf, respectively) are consistent throughout the entire Onaping Formation. The change from greater heterogeneity to homogeneity in Nb/Ta ratio of the Onaping Formation may indeed reflect the change in fragmentation style hypothesised by Grieve et al. (2010) from blocky vitric fragments to lenticular glassy 'green shards'.

A subtle, yet important feature of the HFSE chemostratigraphies is that the ash matrix appears to progress towards a more mafic composition upwards through the Dowling Member. Considering the change in fragmentation style between the Sandcherry Member and the Dowling Member, it is reasonable to propose a gradual change in the relative contributions from felsic towards more mafic sources of melt. The source of the more mafic melt is difficult to ascertain with the present data. It was previously recognised that the contact 'sublayer' below the main mass of the SIC contained material from Huronian tholeiitic basalts and ultramafic enclaves (Lightfoot et al., 1997; Prevec et al., 2000). These could have been assimilated during downward melting of the footwall rocks (Prevec et al., 2000) or, the impact effects may have facilitated tapping into a deep melt source that was immediately mixed with the impact melted target rocks (e.g., Jones et al., 2002). Regardless, the high Nb/Ta and Zr/Hf ratios of the offset dyke and the SIC argue against a separate later addition of a mafic melt (tapped during the change in fragmentation at the Sandcherry–Dowling Member contact) but favour the presence of several melt sources, some possibly at greater lithospheric depth.

5.2.2. The Onaping–Onwatin Formation contact

The apparent increasing influence of mafic products in the Dowling Member ash matrix correlates with a distinct shift in the nature of the deposits, characterised by a pronounced fining upwards and an accompanying increase in percentage of ash matrix. The upper Dowling Member is composed of up to 70% ash matrix by volume (Ames et al., 2006), and grades into the organic-rich shales of the overlying Onwatin Formation. This boundary is widely accepted to represent the transition to a period of quiescence and deep-water deposition within the crater after the termination of the impact-related processes that dominated the Dowling Member sedimentation (Ames et al., 2006; Campos-Alvarez et al., 2010). Petrographically the contact appears gradual, characterised by a decrease in ash and impact melt products and a corresponding increase in organic material and mud particles. However, the contact is very sharply expressed in the HFSE chemostratigraphy. A sudden break in the Nb/Ta and Zr/Hf ratios is found at the boundary (Fig. 3), suggesting that the transition into the Onwatin Formation was abrupt towards values typically exhibited by the UCC. This indicates a complete change in the supply of material to the crater and manner of deposition. In terms of the HFSEs, the boundary denotes a shift towards a source with average Nb/Ta of 14.5 ± 0.5 and an average Zr/Hf of 38.5 ± 0.5. It is important to note at this point that although the homogeneity in refractory elements in the Dowling Member implies reworking and homogenisation throughout the fill sequence, spatial variation in elemental concentrations also occurs. Samples of the Onaping–Onwatin Formation boundary were collected from a drill core taken from the South Range of the crater. In this instance, the Nb/Th ratio (Fig. 3) appears to increase in the upper Dowling Member before returning to average Onaping Formation values in the Onwatin Formation. However, the magnitude of the decrease across the boundary is equivalent to those shown by the Nb/Ta and Zr/Hf ratios. It is reasonable to assume that the Nb/Th ratio of the rest of the Onaping Formation in this region are equally elevated in comparison to the samples collected from the Joe Lake area. Nonetheless, the abrupt shift to lower ratios across the boundary occurs entirely within the core samples, thus the possibility that this decrease at the boundary is simply an artefact of separate sampling locations for the Onaping Formation and the Onwatin Formation can be dismissed.

The initial homogeneity of the middle and upper Dowling Member depicts an isolated environment in which the fuel–coolant interactions and volcanic fragmentation and sedimentation were able to progress for a significant amount of time after the impact without interruption. This constitutes strong evidence for the longevity of the crater integrity, withstanding rim erosion. Eventual disintegration and final collapse of the crater rim would inevitably expose the basin to exogenic input of sediment. The initial input was likely reworked and mixed with the uppermost Dowling Member, indicated by the presence of laminations and cross bedding in the upper half of the Dowling Member and the graded boundary between the two Formations (Ames, 1999; Ames et al., 2006). Furthermore, the rapidity of the change in Nb/Ta and Zr/Hf ratios in the Onwatin Formation over ~200 m of stratigraphy may not solely reflect a sudden change in sediment source but may also have been amplified by slow accumulation rates of incoming muds, which in modern settings can range between 0.001–0.06 m/1000 a to 1 m/1000 a, depending on location and marine input (e.g., Pickering et al., 1989).

Several possible factors were likely a major influence on the initiation and acceleration of the crater disintegration. It is largely agreed that the impact occurred in a shallow sea in a foreland basin of the Penokean orogenic belt (Rousell and Long, 1998; Bunch et al., 1999). The crater structure would also have been subjected to the continuous erosive action of the surrounding ocean. Possible products of erosion found within the Onaping Formation, discussed in Section 5.2.3, could hint at gradual erosion of the exposed crater rim. However, the major breach of the crater walls was likely aided by the deformation of the entire structure under the influence of the Penokean Orogeny, which is partly responsible for the deformation and erosion of the once 150–260 km wide circular structure to a 30×60 km ellipsoid. Thrusting primarily occurred from the modern-day southeast, compressing the Sudbury crater

and aligning the ellipsoid from northeast to southwest. Palaeocurrent data obtained from the Chelmsford Formation, a unit composed largely of turbiditic sandstones and greywackes conformably overlying the Onwatin Formation, indicate major breaches in the crater walls at the two apices causing the preferential flow of material through the resulting large channel (Long, 2004).

5.2.3. Relation of argillites to Onaping and Onwatin Formations

Bunch et al. (1999) first described small, black, fine-grained argillite clasts in the Onaping Formation and interpreted them as shocked fragments of pre-impact, C-rich mudstones. These mudstones were interpreted to have contained kerogen that was proposed to have become reduced to poorly graphitised C upon impact, providing the C that characterises the Dowling Member. The source of the argillite clasts was investigated further by Mungall et al. (2004) with a focus on the PGEs and selected trace elements. It was concluded that the argillites were very similar to the Onaping Formation matrix, and markedly different from both the average crust and the SIC, with the exception that the Ir anomaly that existed in the entire Onaping Formation was absent from the argillite clasts.

In this study, careful hand-picking of matrix provided an opportunity to examine the argillite clasts in detail. Firstly, in terms of physical characteristics, it is interesting to note that the argillite clasts are completely absent from the Sandcherry Member, and only become evident in the Lower Unit of the Dowling Member, decreasing in size and abundance in the Middle and Upper Units. Furthermore, the argillite clasts in the Lower Unit and the Middle Unit are remarkably rounded, unlike most of the fragmented target rocks. It is therefore unlikely that these argillites represent pre-impact carbonaceous rocks as speculated by Bunch et al. (1999), instead suggesting sedimentary transport into the crater, after the deposition of the Sandcherry Member.

In terms of geochemistry, even the most basic comparison of the argillite clasts with the Onaping Formation immediately contradicts the model proposed by Mungall et al. (2004). Most notably, the Zr/Hf ratios of the clasts (ranging from 37.1 to 38.2) are lower than that of the matrix, in the range of typical UCC (37.6, Kamber et al., 2005). Likewise, the Nb/Ta ratios of the clasts (12.2–14.2) are far lower than the matrix (Supplemental Fig. 3A). Both of these ratios suggest a closer affiliation with typical crustally-sourced black shale, such as the Onwatin Formation. In terms of REEs, both Onaping and Onwatin Formation-normalised argillite patterns are relatively flat (Supplemental Fig. 4D), though the clasts are slightly LREE depleted relative to the Onaping Formation matrix.

Whereas the lithophile element ratios indicate similarity between the argillite clasts and the Onwatin Formation, the concentrations of trace metals such as Mo, V, Cr or Co do not. Supplemental Fig. 3D draws attention to the stark contrast between the argillite clasts and both the Onaping Formation and the Onwatin Formation with regard to Mo and V concentrations. The argillite clasts are much lower in Mo and V than the Onaping Formation, and lower still than the Onwatin Formation. The chemistry of the argillites suggest that they formed in a different environment less favourable for the sequestration of Mo and other trace metals.

It can therefore be argued that the clasts are neither target rocks nor pre-existing carbonaceous country rocks. We propose that they were likely deposited and consolidated in the crater but in an area less affected by ongoing impact-related processes and experiencing less juvenile melt input. The argillites were subsequently eroded and transported some distance to the crater floor where they were incorporated into the breccias and tuffs. The decrease in clast size with increasing stratigraphic height is likely a reflection of reworking within the Onaping Formation. Their absence in the Sandcherry Member and Contact Unit of the Dowling Member, and their sudden appearance in the Lower Unit of the Dowling Member suggests that this material was being excluded from the crater during the initial fallback and deposition. We propose that their first appearance might reflect erosion from the depositional environment within the faulted crater rim. Observations from intact craters on Earth and craters on the Moon, Mars and Mercury (e.g., Baker and Head, 2013) strongly suggest that the initially steep interior rim is re-arranged along listric normal faults concentric to the crater rim, where small depositional environments akin to crater-edge half-grabens are formed (e.g., Kenkmann et al., 2014). Thus, in our interpretation, the argillites were transported as erosion products from the crater rim to areas both outside and within the crater, from where they were incorporated into the Onaping Formation.

5.3. Interaction with saline basin water

The presence of water in the Sudbury crater has long been established through petrographic and geochemical evidence, including the operation of an active hydrothermal system (Whitehead et al., 1990; Ames, 1999; Ames et al., 2002; Campos-Alvarez et al., 2010), and the occurrence of extensive zones of peperite in the South Range (Rousell and Brown, 2009). Our chemostratigraphic evidence provides additional insight into the types of interaction with water, and the evolution of the resulting aqueous environment during the deposition of the Onaping and Onwatin Formations.

5.3.1. Trace element and petrographic evidence for interaction with seawater

Recent investigations into the 15 Ma Ries crater in southern Germany has shed new light onto the origin of the Bunte Breccia suevites. There, the impactor targeted a series of Oligocene and Miocene fluvial and lacustrine deposits that overlay Malmian carbonates. After the impact, the karst groundwater system delivered water to the crater, eventually forming a lake that may have persisted for 0.5–2 Ma (Stöffler et al., 2013). Initially, the water flowed onto the melt sheet, promoting "fuel–coolant interactions", propelling melt material into the atmosphere as a plume deposited outside and within the crater (Sheridan and Wohletz, 1983; Stöffler et al., 2013).

In the Sudbury structure, similar violent fuel–coolant interactions between the SIC and the basin water have been

proposed by Grieve et al. (2010) to interpret the changes in internal stratigraphy and lithological characteristics. Studies of water-melt interactions during phreatomagmatic eruptions have found that they can result in blocky, equant shapes in submarine ash deposits (Büttner et al., 1999) that resemble the Equant Shard and Fluidal Fragment units of the Sandcherry Member (Ames et al., 2006).

Supplemental Fig. 1B and C present petrographic evidence of these fuel–coolant interactions in the contact unit of the Dowling Member. The highly vesicular texture of the devitrified clasts suggests that the impact melt from which they formed was high in dissolved volatiles. The serrated appearance of the melt clasts and broken vesicle walls support the hypothesis that cyclical fuel–coolant interactions occurred, whereby the melt instantly vaporizes the fluid it comes into contact with (coolant), forming a vapour film along the surface. The gas bubble expands and implodes suddenly, creating a shockwave through the melt causing fragmentation and generating further surfaces for interaction (Wohletz, 1983; Cas and Giordano, 2014).

Interaction between water and impact melt not only results in macroscopic and petrographic features, but also affects the chemistry of the material. This is most visible in elements that are strongly fractionated between UCC and the dissolved marine inventory. One of the best examples of this in the modern hydrosphere is where the geochemical twins Y and Ho undergo substantial fractionation, resulting in typical seawater Y/Ho ratios of 50–80, twice as high as that of UCC (26.5, Nozaki et al., 1997). Planavsky et al. (2010) demonstrated that the 1.8 Ga ocean already had an elevated non-chondritic Y/Ho ratio. Fig. 5 displays the Y/Ho chemostratigraphy in relation to the vitric rim of the Trill offset dyke. The elevated Ho concentrations within the entire Onaping Formation relative to the offset dyke is easily evident, implying persistent interaction with seawater. The relative elevation in Y content could suggest that either the melt source interacted with seawater or that Y was scavenged from seawater onto the ash particles. In this respect, enrichment of Y in marine ash particles has been reported by Censi et al. (2007) for 2001 eruption products of Mount Etna. It was found that, under alkaline pH conditions, Y forms OH inner-sphere complexes on montmorillonite-type alteration products, decoupling from Ho and causing an increase in Y/Ho in the suspended particle and an anomalously low Y/Ho in the surrounding seawater.

In a similar manner, surface adsorption and colloidal sequestration leads to a very low Th concentration in global oceans relative to U, which is abundant in seawater. Uranium uptake from seawater into particles occurs during alteration, while Th remains constant or decreases during alteration processes (Macdougall et al., 1979; Verma, 1992). The U/Th ratio in the Sandcherry and Dowling Members is elevated to between 0.33 and 0.87, higher than the offset dyke, which has typical UCC values (0.22). This elevation is further evidence of seawater interaction throughout the deposition period after the impact.

Due to the presence of carbonate, the Y/Ho ratios of the Onwatin Formation are elevated to an even greater extent than those of the Onaping Formation, ranging from 29.5 to 33.6. In contrast, the argillite clasts found in the Onaping Formation show Y/Ho ratios equal to their host rocks, indicating that they formed in a separate environment to the Onwatin Formation.

In summary, the Y/Ho and U/Th ratios could be the result of alteration that occurred during the fuel–coolant interactions between the impact melt and the seawater. The violent reactions that caused the shattering and fragmentation of the juvenile clasts and ash matrix may have simultaneously incorporated $Y > Ho$ and $U > Th$ onto alteration products during the quenching of particle rims. Continuous fragmentation would have increased the surface area available for further interaction. In this case, water would have been introduced into the crater very early in crater formation, possibly flooding back into the crater during the collapse of the transient cavity to form the protobasin or peak-ring basin. Alternatively, interaction with seawater may have occurred during the slow settling of ash particles through the water column after initial eruption. This situation may have occurred later, allowing water to seep through the Sandcherry Member and interact with the quenched ash at the same time as the settling ash.

5.3.2. Carbon content and carbon isotope evolution

A persistent question surrounding the Onaping Formation regards the origin and method of emplacement of abundant reduced carbon within the matrix. First noted in reports by Burrows and Rickaby (1930), several explanations have been offered for its existence, however, no consensus has so far been reached. In order to evaluate the source of the C and transport mechanism a systematic study of the relative abundance and isotopic composition of the C throughout the entire fill was conducted.

The original subdivision of the Onaping Formation into the grey member (Sandcherry Member), the green member (Contact Unit of the Dowling Member) and the black member (upper Dowling Member) arose from the distinctive distribution and concentration of C and resultant contrasting colour of each of the units (Muir and Peredery, 1984). The current stratigraphic subdivision of Gibbins et al. (1997) and Ames et al. (1998) was prompted by the discovery that the pattern and distribution of C is independent of the lithological character of the Onaping Formation (Gibbins, 1994). It was therefore implied that the C distribution is not a result of impact processes and deposition, but derived from concomitant processes within or outside of the basin. A previous study by Bunch et al. (1999) reported the occurrence of kerogen in clasts of the upper Dowling Member, but speculated that these had washed in from outside the crater. A biogenic origin for the C of the Whitewater Group has been speculated by many researchers from an early stage (e.g., Williams, 1957; Thomson, 1960; Rousell, 1984), but few detailed chemostratigraphic studies exist.

Decalcified samples from the Joe Lake area revealed an increasing reduced C content from a minimum of ~0.01 wt % in the Sandcherry Member to a maximum of ~0.80 wt% in the Dowling Member (Fig. 6). The uppermost Onaping Formation samples from the drill core have up to

~4.45 wt%C. Previous estimates by Whitehead et al. (1990) found similar maximum concentrations.

The most significant finding from the new data is the coherent chemostratigraphy. It implies that a change in the supply of C occurred. The $\delta^{13}C_{org}$ isotope stratigraphy also portrays this change at the contact (Fig. 6). The highly variable isotopic signatures in the Sandcherry Member and the contact unit of the Dowling Member (ranging from −24.8‰ to −30.8‰) most likely represent either the mixing of target rock lithologies with varying C isotopic values, or the fractionation of light isotopes due to the extreme, but variable temperature and pressure experienced by the target rocks (Mikhail et al., 2014). The distinct shift towards lighter values at the base of the Dowling Member cannot be explained by temperature or pressure changes, and instead marks a change in the origin of the reduced C to a sole source. Samples across the entire Dowling Member show consistently light isotopic values ranging narrowly from −29.2‰ to −31.9‰, which correspond to values typical of Precambrian sedimentary carbonaceous matter (e.g., Hayes et al., 1983), and are indicative of biogenically produced C. These values are within the range previously measured for the Onaping Formation and the Onwatin Formation by Heymann et al. (1999) (−27.1‰ and −35.2‰), but vary on a finer scale. Scatter in the data is likely due to the presence of complex long chain organic material. Whitehead et al. (1990) also reported $\delta^{13}C_{org}$ values of between −29.9‰ and −22.9‰ in the upper Onaping Formation.

The obvious paucity of C in the Sandcherry Member likely reflects an absence of biogenic activity at the time of impact, the initial fallback and melt–coolant interaction; the negligible amounts of C are likely sourced from the limited carbonaceous target rocks and initial surge of seawater into the crater. The progressive increase throughout the Dowling Member implies that either the supply of organic C to the basin greatly increased or the rate of sedimentation in the basin decreased significantly over time. The boundary between the upper Dowling Member and the Onwatin Formation presents a dramatic change in the rate of supply and burial of C to the basin, increasing sharply at the contact to a maximum of ~13% upon termination of the impact related processes and volcanism. Interestingly, the model proposed by Abramov and Kring (2004) suggests that isolated pockets of habitable zones with temperatures of 50–100 °C may have existed in the crater's peripheral regions. These zones may have progressively expanded to a maximum area as the melt sheet cooled towards complete crystallisation after some 200,000 years.

At least in the studied profile at Joe Lake, reduced C and C-isotope distribution is highly systematic. The C-isotope composition argues against carbonaceous matter from a C-chondrite. Although it is accepted that carbon did indeed exist within the target rocks, e.g. because of the presence of impact diamonds in the Onaping Formation (Masaitis et al., 1999), our data do not support the target rock-origin of C proposed by Bunch et al. (1999) and Wright et al. (2010). The consistency of the biogenic isotopic signatures does not reflect a chaotic and energetic emplacement, but rather indicates a single and constant source. Furthermore, the longevity of the crater implied by the lithophile element chemostratigraphies attests to an isolated basin with limited exogenic input of organic C as proposed by Heymann et al. (1999), until the final crater rim collapse. The new data are most consistent with a persisting crater basin filled with water and inhabited by microbial life.

5.3.3. Redox state

From the perspective of impact craters as possible habitats of life, it matters whether C was produced within the basin or was transported there from an external site. The scenario from the lithophile element analysis is that of a submarine impact crater, whose rim stayed emerged beyond the sea surface for a significant period of time. Thus, the water within the basin would not have been in full communication with the open ocean. This hypothesis can be further tested with redox-sensitive metals, such as Mo, V, U, Cr, Co and Cu, whose behaviour in the ocean depends on redox state and depositional environment.

Before analysing the metal data, it is worth re-iterating that the impact likely occurred in a foreland basin and not the open ocean (e.g., Rousell and Long, 1998). Thus, the crater rim heights predicted by numerical models (ca. 1–2 km; Collins et al., 2005) for craters on the order of 200 km in diameter are entirely consistent with the idea that the rim of the crater was exposed to the atmosphere and contained a restricted basin, even taking into account that much of the rim would have collapsed into the basin along normal faults. The persistent preservation of organic C up stratigraphy of the Onaping Formation alone suggests that a prolonged period of anoxia occurred in the basin.

The following discussion will focus on the elements Mo and U whose utility as environmental indicators is based on their high modern marine enrichment over crustal abundances and their specific environmentally-controlled behaviours (e.g., Richards, 1975; Morford and Emerson, 1999). The authigenic concentrations of these elements in oceanic sediments are particularly interesting in the context of silled or otherwise restricted basins (Algeo and Tribovillard, 2009). In the Onaping Formation, both metals show striking chemostratigraphies with very well-developed topographies (Fig. 7). Relatively high concentrations of elements such as Mo, Co, V and Ni in the Onaping Formation relative to the country rocks had been noted previously by Speers (1957) but not in the context of chemostratigraphy.

The stratigraphic evolution of the Mo enrichment factor (MoEF, Algeo and Tribovillard, 2009) throughout the Onaping Formation appears to have occurred in five stages (Fig. 8). Firstly, through the top of the Sandcherry Member and into the Contact Unit, Mo enrichment is erratic, ranging from depletion relative to the offset dyke composition to quite strong enrichment. We attribute this to heterogeneous contribution of lithic clasts to the hand-picked matrix, as well as reflecting the chaotic nature of the Sandcherry Member. Higher Mo concentrations are expected via contributions from the ubiquitous mafic targets (e.g., Petrus et al., 2015a). The Mo concentration in the Sandcherry Member may additionally have been influenced by partial loss due to vaporisation (alongside Pb and Sb).

Regardless, the second stage commenced with the subsequent rapid increase in the authigenic concentration of Mo in the Lower Unit of the Dowling Member simultaneous with the sudden increase of organic carbon burial at this point due to crater collapse (Figs. 6 and 7). It is likely that the sudden input of organic C caused the rapid adsorption of Mo onto settling organic particles (Scott et al., 2008), which were then buried alongside the ash matrix. Thus, by analogy with modern anoxic basins, we postulate that the build-up of reduced C in the stagnant crater basin may have led to anoxic and euxinic conditions that favoured the mineralisation of Mo.

The third stage is represented by the long stratigraphic interval represented by the Lower, Middle and Upper Units of the outcrop samples of the Dowling Member (thus excluding the uppermost Upper Unit represented by the core samples). In these samples, both absolute Mo concentration and MoEF declined with time. The important observation in this regard is that across the entire suite of Dowling Member outcrop samples, there is a lack of correlation ($r^2 = 0.16$, Fig. 9B) between TOC and MoEF. This observation could have several explanations. Firstly, it could reflect a change from euxinic towards ferruginous conditions up stratigraphy. Secondly, it could imply the onset of a reservoir effect caused by the partial exhaustion of the available pool of molybdates in the restricted crater basin. Finally, it could imply a decline in hydrothermal Mo input into the basin, possibly related to the abundance of large individual pyroclastic units (Ames et al., 2006).

The fourth stage is represented by the very top of the Upper Unit of the Dowling Member where both Mo concentrations and MoEF rapidly increased. They remained elevated in the samples from the Onwatin Formation which, however, are more enriched in V (Fig. 7) and represent the final fifth stage. In the context of the constraints from the HFSE, which indicate that the sediment in the mudstones of the Onwatin Formation was sourced from outside the basin, it appears logical to propose that stage 4 represents the breach of the rim by surrounding seawater, at a time when sediment was still excluded from entering the basin. The resulting influx of open seawater either changed basin conditions and/or supplied Mo and sulphate to greatly increase Mo mineralisation. By stage 5, the mudstones of the Onwatin Formation were being deposited and the basin was certainly in communication with the surrounding ocean.

We used the approach of Algeo and Tribovillard (2009) to test the possibility of a reservoir effect causing stage 3. This method involves plotting the EFs of Mo and U against each other (Fig. 9A). In the resulting diagram, it is possible to distinguish depositional centers above zones of nutrient upwelling on account of their very high UEF at relatively modest MoEF. By contrast, silled basins with euxinic conditions plot at high MoEF but low UEF. Restricted and strongly restricted basins that experience reservoir effects plot in between. Although neither the U nor the Mo content of the 1.85 Ga ocean is known, we note that the Dowling Member samples cluster in the same area as sediments from the Black Sea, a modern restricted basin (Algeo and Tribovillard, 2009). It is evident that with increasing stratigraphic height, the MoEF in the Dowling Member diminished at slightly increasing UEF, supporting the notion that Mo may have become supply-limited, thereby explaining the lack of correlation of Mo with TOC (Fig. 9B). Regardless of the limitations of this comparison with the modern ocean, it is clear that there was a significant shift towards higher MoEF/UEF during stage 4. The uppermost Dowling Member samples and the Onwatin Formation mudstones plot into the same area as modern silled basins in the open ocean above zones of nutrient upwelling. The interpretation of re-supply of basin water and molybdates from the surrounding ocean is further supported by the high degree of correlation ($r^2 = 0.88$; not shown) between TOC and MoEF of the entire dataset (Emerson and Huested, 1991). In this interpretation, stage 3 represents an enclosed crater basin with limited exchange of water from the surrounding ocean, followed by stage 4 where fresh seawater flooded into the basin, finally leading to stage 5, during which the crater wall was fully submerged. This last transition may also be reflected in the sharp increase in VEF from the uppermost Dowling Member samples into the Onwatin Formation.

An additional thin horizon, which was not analysed in this study is the economically important Vermilion Formation, composed of discontinuous carbonate rocks hosting significant volcanic massive sulphide (VMS) deposits found between the Onaping and Onwatin Formations. The Vermilion Formation, along with abundant but less economic hydrothermal deposits at the SIC-Onaping interface and sparse hydrothermal deposits throughout the Contact, Lower and Middle Units of the Dowling Member C (Ames et al., 2002), has been interpreted as evidence for a hydrothermal system that prevailed throughout the deposition of the Sandcherry Member and part of the Dowling Member (Ames et al., 1998, Ames et al., 2006). Given the new evidence for abundant subaqueous volcanism prevailing throughout the entire Dowling Member (such as hydroclastic fractured clasts in the uppermost Dowling Member, Ames et al., 2002), it is interesting that this extremely well-defined horizon precisely coincides with the change in sedimentation and the breach of the crater walls, both occurring at the end of the volcanic activity. It is possible that during stage 3, the crater basin became depleted in sulphate due to the same reservoir effect that depleted Mo, starving the hydrothermal systems in S. As fresh seawater, high in sulphate, flowed into the basin at the end of volcanic activity during stage 4, the final sulphate-loaded hydrothermal systems deposited sharply defined VMS horizons. By stage 5, volcanic and hydrothermal activity had largely ceased and no further VMS deposits could form.

5.4. Working model

Contrary to previous studies, which concluded that the Onaping Formation is largely composed of reworked impact melt, the new chemostratigraphic data preserve coherent trends that can be interpreted with a post-impact evolutionary model, with implications for the sustainability of life in the crater. The proposed working hypothesis for

the development of the post-impact environment can be broken down into three stages (Fig. 10).

Immediately following the impact, crater modification in response to rebound of the transient cavity created a multi-ring circular crater with a final diameter of between 150 and 260 km, within which shock melt had pooled. The melt sheet eventually crystallised into what is now the SIC. The collapse of the primary ejecta plume deposited a thin (a few tens of metres) fallback layer of fragmented target rocks, primary impact melt and ash. Early in its evolution, the crater experienced an influx of seawater, either during the collapse of the transient cavity under the surface of the ocean, by impact-related tsunamis surging over the crater rim, or by seepage through the faulted crater walls. The seawater encountered very hot and possibly superheated fallback material and the melt sheet, leading to violent melt–coolant type interactions that formed the breccias of the Sandcherry Member. Thus, the Sandcherry Member is largely the result of the catastrophic collapse and faulting of the initial crater and deposits already contained within, and is composed of reworked impact melt and lithic clasts. Either as a consequence of the extreme temperatures experienced during shock melting and/or because of the melt–water interaction, certain volatile elements were lost to the atmosphere. What little reduced C was incorporated into the breccias does not have a clear biogenic isotope composition. Once the top of the melt sheet had cooled sufficiently, seawater started to fill the crater but the crater rim continued to protrude above the surface of the ocean, isolating the basin.

There is clear evidence for structural discontinuities between the Sandcherry and Dowling Members and the resultant palaeo-topography at the contact was eventually filled with the deposits of the Contact and Lower Units of the Dowling Member. These units contain bombs, blocks and an abundance of green, cm- to dm-sized angular vitric shards, indicating that extensive volcanic activity was initiated at the Sandcherry–Dowling Member boundary. Most volcanic products were emplaced under water. Up stratigraphy, the size of the products gradually diminished and ash-sized matrix became the dominant component of the tuffs. The chemistry of the matrix clearly indicates that the main source of material was very similar to the impact melt. The very gradual decline in subaqueous explosive volcanic activity is mirror-imaged by the increase in organic C content that was being deposited. The C isotope composition is compatible with the idea that prokaryotic extremophile plankton colonised the basin, a new habitat in which their population expanded. The resulting organic rain-down onto the developing Dowling Member sustained an anoxic–euxinic water column from which elements such as Mo were sequestered.

The lack of linear increase between the concentrations of redox-sensitive metals such as V and Mo with reduced C content suggests that either a metal reservoir effect was encountered or the sulphate concentration in the basin was gradually reduced, leading to anoxic but non-euxinic conditions. It is noteworthy that concordant hydrothermal VMS-deposits occur within the Dowling Member. VMS deposits are typically associated with mid-ocean ridges but the Sudbury basin shows that similar hydrothermal systems can also occur in impact basins. Thus, the link between generation of building blocks of life and hydrothermal systems associated with plate spreading (e.g., Martin et al., 2008; Russell et al., 2010) may need to be revisited. In the outer reaches of the multi-ring structure, argillaceous muds devoid of volcanic components were being deposited. These were transported into the basin and incorporated into the Dowling Member as the rim began to succumb to erosion.

Ongoing deformation related to the Penokean Orogeny likely compromised the integrity of the structure, initiating the collapse of the crater walls. Breach of the crater likely occurred at the apices of the resulting ellipse, re-establishing communication with the open ocean. The sudden flooding of the basin with seawater replenished the exhausted basin with nutrients (sulphate) and transition metals, prompting a period of prokaryotic productivity. Volcanic and hydrothermal activity persisted to this point. However, the crater may have become too starved in sulphate in the uppermost Dowling Member to permit operation of effective VMS systems until communication with the open sea was established, allowing a sudden, short-lived period of VMS deposition.

Volcanic activity ceased shortly after, and a period of quiescence allowed the slow accumulation of organic matter and mud particles to construct the Onwatin Formation. The chemistry of the mudstones clearly shows that by now, sediment was being sourced from outside the crater. Deformation continued to influence the shape of the crater, and the resultant submarine NNW-SSE valley became a conduit for turbulent flows, finally depositing the greywackes and sandstones of the uppermost crater fill, the Chelmsford Formation.

6. CONCLUSIONS

Very large to giant impact events undoubtedly were amongst the most significant factors controlling the habitability of the early Earth. Consequences of Hadean impacts include the possibility of repeated sterilization of the Earth's surface, the energetic delivery of materials, including complex organic molecules from meteorites and comets, and the provision of enclosed, spatially restricted environments within the resulting crater rims. The sparse geological and isotopic data relevant to the Hadean suggest that the Earth was already encased in a hydrosphere (e.g., Valley et al., 2002; Kramers, 2003). Therefore, many Hadean impacts may have hit subaqueous targets. Observations from the Moon, Mars and Mercury are exclusively from impact sites on land. By contrast, the present study reports the first detailed chemostratigraphic reconstruction of the lower basin fill (the Onaping Formation) of the largest preserved and accessible subaqueous terrestrial impact crater.

The Sudbury impact crater is unique among the known impact structures on Earth. Its size, complexity, subaqueous nature, and accessibility make it an important analogue candidate for structures created during the Hadean and Eoarchaean. Our detailed chemostratigraphies suggest that very large impact basins in relatively shallow water may

have provided isolated submarine environments in which violent melt–coolant type interaction occurred. In the case of the Sudbury structure, these initial violent reactions between the SIC and inflowing seawater produced the breccias of the Sandcherry Member. The immense heat of the impact and the initial melt–water interaction caused the loss of several volatile elements from the early deposits to the atmosphere. Continued interaction between the melt sheet and seawater, and possible volcanic activity on the crater floor caused the subsequent buildup of the Onaping Formation, and the establishment of an active hydrothermal system within the basin. As the volcanic activity began to diminish and temperatures declined within the basin, life began to proliferate in the surface waters, incorporating organic material into the Dowling Member ash. Isolation from the surrounding ocean caused the chemistry of the crater basin to evolve and induced a reservoir effect, being influenced by factors such as sequestration of redox-sensitive metals associated with decaying organic matter, delivery of heat and nutrients from hydrothermal systems, and alteration of volcanic glass. This reservoir effect led to a period of anoxia and possibly euxinia within the basin, interrupted only as the crater rim began to collapse and caused an influx of fresh seawater to enter the basin, allowing life to bloom. Isolated impact basins may therefore have provided individual microenvironments of more varied nature than a single open ocean, increasing the likelihood for establishment of life.

ACKNOWLEDGEMENTS

This research was funded by Science Foundation Ireland grant SFI/12/ERC/E2499 awarded to B.S.K. We would like to thank Chris Caron for helping us access the drill core and Glencore (Lucy Potter) for making the core available for this study. Many thanks also to Joseph Petrus for providing a batch of Onaping Formation samples. We would like to express our thanks to Lindsay Hall from the Canadian Institute for Mining, Metallurgy and Petroleum for sharing her expertise in field geology. We acknowledge the help and support of Dr. Teresa Ubide, Gavin Kenny and Paul Guyett for fieldwork and sample collection assistance, and to Cora McKenna and Dr. Michael Babechuk for technical support during ICP-MS analysis. Finally, two constructive reviews (by Michael Lesher and anonymous) and the helpful editorial suggestions by Christian Koeberl are acknowledged.

APPENDIX A. SUPPLEMENTARY DATA

Supplementary data associated with this article can be found, in the online version, at http://dx.doi.org/10.1016/j.gca.2016.04.007.

REFERENCES

Abramov O. and Kring D. A. (2004) Numerical modelling of an impact-induced hydrothermal system at the Sudbury crater. *J. Geophys. Res.* **109**. http://dx.doi.org/10.1029/2003JE002213.

Addison W. D., Brumpton G. R., Davis D. W., Fralick P. W. and Kissin S. A. (2010) Debrisites from the Sudbury impact event in Ontario, north of Lake Superior, and a new age constraint: are they base-surge deposits or tsunami deposits? In *Large Meteorite Impacts and Planetary Evolution IV*, 465 (eds. R. L. Gibson and W. U. Reimold), pp. 245–268. Geol. Soc. Am. Spec. Pap..

Addison W. D., Brumpton G. R., Vallini D. A., Mcnaughton N. J., Davis D. W., Kissin S. A., Fralick P. W. and Hammond A. L. (2005) Discovery of distal ejecta from the 1850 Ma Sudbury impact event. *Geology* **33**, 193–196.

Algeo T. J. and Lyons T. W. (2006) Mo–total organic carbon covariation in modern anoxic marine environments: implications for analysis of paleoredox and paleohydrographic conditions. *Paleoceanography* **21**. http://dx.doi.org/10.1029/2004PA001112.

Algeo T. J. and Tribovillard N. (2009) Environmental analysis of paleoceanographic systems based on molybdenum–uranium covariation. *Chem. Geol.* **268**, 211–225.

Allegre C. J. (1968) Comportement Des Systemes U–Th–Pb Dans Le Manteau Superieur Et Modele d'Evolution De Ce Dernier Au Cours Des Temps Geologiques. *Earth Planet. Sci. Lett.* **5**, 261–269.

Alvarez L. W., Alvarez W., Asaro F. and Michel H. V. (1980) Extraterrestrial cause for the cretaceous-tertiary extinction. *Science* **208**, 1095–1108.

Ames D. E., Watkinson D. H. and Parrish R. R. (1998) Dating of a regional hydrothermal system induced by the 1850 Ma Sudbury impact event. *Geology* **26**, 447–450.

Ames D. E. (1999) Geology and regional hydrothermal alteration of the crater-fill, Onaping Formation: association with Zn–Pb–Cu mineralization, Sudbury structure, Canada Ph. D. thesis. Carleton Univ..

Ames D., Gibson H. and Watkinson D. (2000) Controls on major impact-induced hydrothermal system, Sudbury Structure, Canada. *Lunar Planet. Sci. XXXI*. Lunar Planet. Inst., Houston. #1873 (abstr.).

Ames D. E., Golightly J. P., Lightfoot P. C. and Gibson H. L. (2002) Vitric compositions in the Onaping Formation and their relationship to the Sudbury igneous complex, Sudbury structure. *Econ. Geol.* **97**, 1541–1562.

Ames D. E. and Gibson H. L. (2004) Geology, Alteration and Mineralization of the Onaping Formation, Joe Lake area, Wisner Township, Sudbury Structure, Ontario. Geological Survey of Canada, Open file 4566. Scale 1:2000.

Ames D. E., Jonasson I. R., Gibson H. L. and Pope K. O. (2006) Impact-generated hydrothermal system—constraints from the large paleoproterozoic Sudbury Crater, Canada. In *Biological Processes Associated with Impact Events* (eds. C. Cockell, I. Gilmour and C. Koeberl). Springer, Berlin Heidelberg, pp. 55–100.

Arevalo, Jr., R. and McDonough W. F. (2010) Chemical variations and regional diversity observed in MORB. *Chem. Geol.* **271**, 70–85.

Asael D., Tissot F. L. H., Reinhard C. T., Rouxel O., Dauphas N., Lyons T. W., Ponzevera E., Liorzou C. and Chéron S. (2013) Coupled molybdenum, iron and uranium stable isotopes as oceanic paleoredox proxies during the Paleoproterozoic Shunga Event. *Chem. Geol.* **362**, 193–210.

Babechuk M. G., Kamber B. S., Greig A., Canil D. and Kodolányi J. (2010) The behaviour of tungsten during mantle melting revisited with implications for planetary differentiation time scales. *Geochim. Cosmochim. Acta* **74**, 1448–1470.

Babechuk M. G., Widdowson M. and Kamber B. S. (2014) Quantifying chemical weathering intensity and trace element release from two contrasting basalt profiles, Deccan Traps, India. *Chem. Geol.* **363**, 56–75.

Baker D. M. H. and Head J. W. (2013) New morphometric measurements of craters and basins on Mercury and the Moon from MESSENGER and LRO altimetry and image data: an

observational framework for evaluating models of peak-ring basin formation. *Planet. Space Sci.* **86**, 91–116.
Baross J. A. and Hoffman S. E. (1985) Submarine hydrothermal vents and associated gradient environments as sites for the origin and evolution of life. *Origins Life. Evol. Biosph.* **15**, 327–345.
Barth M. G., McDonough W. F. and Rudnick R. L. (2000) Tracking the budget of Nb and Ta in the continental crust. *Chem. Geol.* **165**, 197–213.
Bau M. and Dulski P. (1999) Comparing yttrium and rare earths in hydrothermal fluids from the Mid-Atlantic Ridge: implications for Y and REE behaviour during near-vent mixing and for the Y/Ho ratio of Proterozoic seawater. *Chem. Geol.* **155**, 77–90.
Bunch T. E., Becker L., Marais D., Tharpe A., Schultz P. H., Wolbach W., Glavin D. P., Brinton K. L. and Bada J. L. (1999) Carbonaceous matter in the rocks of the Sudbury Basin, Ontario, Canada. *Geol. Soc. Am. Spec. Pap.*, 331–344.
Burrows A. and Rickaby H. (1930). *Sudbury basin area*.
Büttner R., Dellino P. and Zimanowski B. (1999) Identifying magma–water interaction from the surface features of ash particles. *Nature* **401**, 688–690.
Byrne R. H. and Lee J. H. (1993) Comparative yttrium and rare earth element chemistries in seawater. *Mar. Geol.* **44**, 121–130.
Campos-Alvarez N. O., Samson I. M., Fryer B. J. and Ames D. E. (2010) Fluid sources and hydrothermal architecture of the Sudbury Structure: constraints from femtosecond LA-MC-ICP-MS Sr isotopic analysis of hydrothermal epidote and calcite. *Chem. Geol.* **278**, 131–150.
Cas R. A. F. and Giordano G. (2014) Submarine volcanism: a review of the constraints, processes and products, and relevance to the Cabo de Gata volcanic succession. *Ital. J. Geosci.* **133**, 362–377.
Censi P., Sprovieri M., Larocca D., Aricò P., Saiano F., Mazzola S. and Ferla P. (2007) Alteration effects of volcanic ash in seawater: anomalous Y/Ho ratios in coastal waters of the Central Mediterranean sea. *Geochim. Cosmochim. Acta* **71**, 5405–5422.
Chyba C. F., Thomas P. J., Brookshaw L. and Sagan C. (1990) Cometary delivery of organic molecules to the early earth. *Science* **249**, 366–373.
Cloëz S. (1864) Analyse chimique de la pierre météorique d'Orgueil. *C.R. Acad. Sci.* **59**, 37–40.
Collins G. S., Melosh H. J. and Marcus R. A. (2005) Earth Impact Effects Program: a web-based computer program for calculating the regional environmental consequences of a meteoroid impact on Earth. *Meteorit. Planet. Sci.* **40**, 817–840.
Dam G., Pedersen G. K., Sønderholm M., Midtgaard H. H., Larsen L. M., Nøhr-Hansen H. and Pedersen A. K. (2009). *Lithostratigraphy of the Cretaceous-Paleocene Nuussuaq Group, Nuussuaq Basin, West Greenland*.
Daniel I., Oger P. and Winter R. (2006) Origins of life and biochemistry under high-pressure conditions. *Chem. Soc. Rev.* **35**, 858–875.
Darling J. R., Hawkesworth C. J., Lightfoot P. C., Storey C. D. and Tremblay E. (2010b) Isotopic heterogeneity in the Sudbury impact melt sheet. *Earth Planet. Sci. Lett.* **289**, 347–356.
Darling J. R., Hawkesworth C. J., Storey C. D. and Lightfoot P. C. (2010a) Shallow impact: isotopic insights into crustal contributions to the Sudbury impact melt sheet. *Geochim. Cosmochim. Acta* **74**, 5680–5696.
David K., Schiano P. and Allègre C. J. (2000) Assessment of the Zr/Hf fractionation in oceanic basalts and continental materials during petrogenetic processes. *Earth Planet. Sci. Lett.* **178**, 285–301.
Dietz R. S. (1964) Sudbury structure as an astrobleme. *J. Geol.* **72**, 412–434.
Dressler B. O., Weiser T. and Brockmeyer P. (1996) Recrystallized impact glasses of the Onaping formation and the Sudbury igneous Complex, Sudbury Structure, Ontario, Canada. *Geochim. Cosmochim. Acta* **60**, 2019–2036.
Ebert M., Hecht L., Deutsch A., Kenkmann T., Wirth R. and Berndt J. (2014) Geochemical processes between steel projectiles and silica-rich targets in hypervelocity impact experiments. *Geochim. Cosmochim. Acta* **133**, 257–279.
Elkins-Tanton L. T., Hager B. H. and Grove T. L. (2004) Magmatic effects of the lunar late heavy bombardment. *Earth Planet. Sci. Lett.* **222**, 17–27.
Emerson S. R. and Huested S. S. (1991) Ocean anoxia and the concentrations of molybdenum and vanadium in seawater. *Mar. Geol.* **34**, 177–196.
Ehrenfreund P., Glavin D. P., Botta O., Cooper G. and Bada J. L. (2001) Extraterrestrial amino acids in Orgueil and Ivuna: tracing the parent body of CI type carbonaceous chondrites. *Proc. Natl. Acad. Sci. U.S.A.* **98**, 2138–2141.
Fedo C. M., Nesbitt H. W. and Young G. M. (1995) Unraveling the effects of potassium metasomatism in sedimentary rocks and paleosols, with implications for paleoweathering conditions and provenance. *Geology* **23**, 921–924.
French B. M. (1970) Possible relations between meteorite impact and igneous petrogenesis, as indicated by the Sudbury structure, Ontario, Canada. *Bull. Volcanol.* **34**, 466–517.
Gibbins S. (1994) *Geology, Geochemistry, Stratigraphy and Mechanisms of Emplacement of the Onaping Formation, Dowling Area, Sudbury Structure, Ontario Canada*. Laurentian University, Sudbury, Ontario.
Gibbins S., Gibson H., Ames D. E. and Jonasson I. (1997) The Onaping Formation: stratigraphy, fragmentation, and mechanisms of emplacement. In *Proceedings of the Conference on Large Meteorite Impacts and Planetary Evolution: Sudbury*. LPI contribution #922, Lunar Planet. Inst., Houston. 16 (abstr.).
Goesmann F., Rosenbauer H., Bredehöft J. H., Cabane M., Ehrenfreund P., Gautier T., Giri C., Krüger H., Le Roy L., Macdermott A. J., Mckenna-Lawlor S., Meierhenrich U. J., Caro G. M. M., Raulin F., Roll R., Steele A., Steininger H., Sternberg R., Szopa C., Thiemann W. and Ulamec S. (2015) Organic compounds on comet 67P/Churyumov-Gerasimenko revealed by COSAC mass spectrometry. *Science* **349**. http://dx.doi.org/10.1126/science.aab0689.
Green T. H. (1995) Significance of Nb/Ta as an indicator of geochemical processes in the crust–mantle system. *Chem. Geol.* **120**, 347–359.
Grieve R. A. F. (1994) An impact model of the Sudbury structure. In *Proceedings of the Sudbury-Noril'sk Symposium*, 5 (eds. P. C. Lightfoot and A. J. Naldrett), pp. 119–132. Ontario Geological Survey Special.
Grieve R. A. F., Stöffler D. and Deutsch A. (1991) The Sudbury structure-controversial or misunderstood? *J. Geophys. Res.* **96**, 753-722.
Grieve R. A. F., Ames D. E., Morgan J. V. and Artemieva N. (2010) The evolution of the Onaping Formation at the Sudbury impact structure. *Meteorit. Planet. Sci.* **45**, 759–782.
Hayes J., Wedeking K. and Kaplan I. (1983) Precambrian organic geochemistry – preservation of the record. In *Earth's Earliest Biosphere: Its Origin and Evolution* (ed. H. W. Schopf). Princeton Univ. Press, Princeton, pp. 93–134.
Heymann D., Dressier B., Knell J., Thiemens M., Buseck P., Dunbar R. and Mucciarone D. (1999) Origin of carbonaceous matter, fullerenes, and elemental sulfur in rocks of the Whitewater Group, Sudbury impact structure, Ontario, Canada. In *Large Meteorite Impacts and Planetary Evolution II*, 339 (eds. B. O. Dresslar and V. L. Sharpton), pp. 345–360. Geological Society of America.

Hirt A. M., Lowrie W., Clendenen W. S. and Kligfield R. (1993) Correlation of strain and the anisotropy of magnetic susceptibility in the Onaping Formation: evidence for a near-circular origin of the Sudbury Basin. *Tectonophysics* **225**, 231–254.

Jones A. P., Price G. D., Price N. J., Decarli P. S. and Clegg R. A. (2002) Impact induced melting and the development of large igneous provinces. *Earth Planet. Sci. Lett.* **202**, 551–561.

Kamber B. S., Ewart A., Collerson K., Bruce M. and McDonald G. (2002) Fluid-mobile trace element constraints on the role of slab melting and implications for Archaean crustal growth models. *Contrib. Mineral. Petrol.* **144**, 38–56.

Kamber B. S., Greig A. and Collerson K. D. (2005) A new estimate for the composition of weathered young upper continental crust from alluvial sediments, Queensland, Australia. *Geochim. Cosmochim. Acta* **69**, 1041–1058.

Keller G., Adatte T., Stinnesbeck W., Rebolledo-Vieyra M., Urrutia Fucugauchi J., Kramar U. and Stüben D. (2004) Chicxulub impact predates the K-T boundary mass extinction. *Proc. Natl. Acad. Sci. USA* **101**, 3753–3758.

Kelley D. S., Karson J. A., Früh-Green G. L., Yoerger D. R., Shank T. M., Butterfield D. A., Hayes J. M., Schrenk M. O., Olson E. J., Proskurowski G., Jakuba M., Bradley A., Larson B., Ludwig K., Glickson D., Buckman K., Bradley A. S., Brazelton W. J., Roe K., Elend M. J., Delacour A., Bernasconi S. M., Lilley M. D., Baross J. A., Summons R. E. and Sylva S. P. (2005) A serpentinite-hosted ecosystem: the lost city hydrothermal field. *Science* **307**, 1428–1434.

Kenkmann T., Poelchau M. H. and Wulf G. (2014) Structural geology of impact craters. *J. Struct. Geol.* **62**, 156–182.

Kimura K., Lewis R. S. and Anders E. (1974) Distribution of gold and rhenium between nickel-iron and silicate melts: implications for the abundance of siderophile elements on the Earth and Moon. *Geochim. Cosmochim. Acta* **38**, 683–701.

Kleine T. (2011) Geoscience: Earth's patchy late veneer. *Nature* **477**, 168–169.

Kramers J. D. (2003) Volatile element abundance patterns and an early liquid water ocean on Earth. *Precambrian Res.* **126**, 379–394.

LaFrance B. and Kamber B. S. (2010) Geochemical and microstructural evidence for in situ formation of pseudotachylitic Sudbury breccia by shock-induced compression and cataclasis. *Precambrian Res.* **180**, 237–250.

Lagos M., Ballhaus C., Munker C., Wohlgemuth-Ueberwasser C., Berndt J. and Kuzmin D. V. (2008) The Earth's missing lead may not be in the core. *Nature* **456**, 89–92.

Lazcano A., Oro J. and Miller S. L. (1983) Primitive Earth environments: organic syntheses and the origin and early evolution of life. *Precambrian Res.* **20**, 259–282.

Lightfoot P. C. and Doherty W. (2001) Chemical evolution and origin of nickel sulfide mineralization in the Sudbury igneous complex, Ontario, Canada. *Econ. Geol.* **96**, 1855–1875.

Lightfoot P. C., Keays R. R., Morrison G. G., Bite A. and Farrell K. P. (1997) Geochemical relationships in the Sudbury igneous complex; origin of the main mass and offset dikes. *Econ. Geol.* **92**, 289–307.

Lightfoot P. C. (1997) *Geochemistry of the Main Mass, Sublayer, Offsets, and Inclusions from the Sudbury Igneous Complex, Ontario* Ontario Geological Survey Open File Report 5959, p. 231.

Long D. G. F. (2004) The tectonostatigraphic evolution of the Huronian basement and the subsequent basin fill: geological constraints on impact models of the Sudbury event. *Precambrian Res.* **129**, 203–223.

Lowe D. R. and Byerly G. R. (2015) Geologic record of partial ocean evaporation triggered by giant asteroid impacts, 3.29–3.23 billion years ago. *Geology* **43**, 535–538.

Macdougall J. D., Finkel R. C., Carlson J. and Krishnaswami S. (1979) Isotopic evidence for uranium exchange during low-temperature alteration of oceanic basalt. *Earth Planet. Sci. Lett.* **42**, 27–34.

Maher K. A. and Stevenson D. J. (1988) Impact frustration of the origin of life. *Nature* **331**, 612–614.

Maier W. D., Barnes S. J., Campbell I. H., Fiorentini M. L., Peltonen P., Barnes S.-J. and Smithies R. H. (2009) Progressive mixing of meteoritic veneer into the early Earth's deep mantle. *Nature* **460**, 620–623.

Martin W., Baross J., Kelley D. and Russell M. J. (2008) Hydrothermal vents and the origin of life. *Nat. Rev. Microbiol.* **6**, 805–814.

Masaitis V. L., Shafranovsky G. I., Grieve R. A. F., Langenhorst F., Peredery W. V., Therriault A. M., Balmasov E. L. and Fedorova I. G. (1999) Impact diamonds in the Suevitic Breccias of the Black Member of the Onaping Formation, Sudbury Structure, Ontario, Canada. *Geol. Soc. Am. Special Papers* **339**, 317–321.

McLennan S. M. (2001) Relationships between the trace element composition of sedimentary rocks and upper continental crust. *Geochem. Geophys. Geosyst.* **2**. http://dx.doi.org/10.1029/2000GC000109.

Mikhail S., Guillermier C., Franchi I. A., Beard A. D., Crispin K., Verchovsky A. B., Jones A. P. and Milledge H. J. (2014) Empirical evidence for the fractionation of carbon isotopes between diamond and iron carbide from the Earth's mantle. *Geochem. Geophys. Geosyst.* **15**, 855–866.

Miller D. M., Goldstein S. L. and Langmuir C. H. (1994) Cerium/lead and lead isotope ratios in arc magmas and the enrichment of lead in the continents. *Nature* **368**, 514–520.

Morbidelli A., Chambers J., Lunine J., Petit J., Robert F., Valsecchi G. and Cyr K. (2000) Source regions and time scales for the delivery of water to Earth. *Meteorit. Planet. Sci.* **35**, 1309–1320.

Morford J. L. and Emerson S. (1999) The geochemistry of redox sensitive trace metals in sediments. *Geochim. Cosmochim. Acta* **63**, 1735–1750.

Muir T. (1984) The Sudbury structure: considerations and models for an endogenic origin. In *The Geology and Ore Deposits of the Sudbury Structure*, 1 (eds. E. G. Pye, A. J. Naldrett and P. E. Giblin), pp. 449–489. Ontario Geological Survey, Special.

Muir T. and Peredery W. (1984) The Onaping formation. In *The Geology and Ore Deposits of the Sudbury Structure*, 1 (eds. E. G. Pye, A. J. Naldrett and P. E. Giblin), pp. 139–210. Ontario Geological Survey, Special.

Mungall J. E., Ames D. E. and Hanley J. J. (2004) Geochemical evidence from the Sudbury structure for crustal redistribution by large bolide impacts. *Nature* **429**, 546–548.

Münker C., Pfänder J. A., Weyer S., Büchl A., Kleine T. and Mezger K. (2003) Evolution of planetary cores and the Earth–Moon system from Nb/Ta systematics. *Science* **301**, 84–87.

Naldrett A. J., Bray J. G., Gasparrini E. L., Podolsky T. and Rucklidge J. C. (1970) Cryptic variation and petrology of the Sudbury nickel irruptive. *Econ. Geol.* **65**, 122–155.

Nemchin A. A., Whitehouse M. J., Grange M. L. and Muhling J. R. (2011) On the elusive isotopic composition of lunar Pb. *Geochim. Cosmochim. Acta* **75**, 2940–2964.

Nesbitt H. W. and Young G. M. (1982) Early Proterozoic climates and plate motions inferred from major element chemistry of lutites. *Nature* **299**, 715–717.

Nozaki Y., Zhang J. and Amakawa H. (1997) The fractionation between Y and Ho in the marine environment. *Earth Planet. Sci. Lett.* **148**, 329–340.

O'Neill H. S. C. and Palme H. (2008) Collisional erosion and the non-chondritic composition of the terrestrial planets. *Philos. Trans. R. Soc. A.* **366**, 4205–4238.

Peredery W. and Morrison G. (1984) Discussion of the origin of the Sudbury Structure. In *The Geology and Ore Deposits of the Sudbury Structure*, 1 (eds. E. G. Pye, A. J. Naldrett and P. E. Giblin), pp. 491–511. Ontario Geological Survey, Special.

Petrus J. A., Ames D. E. and Kamber B. S. (2015a) On the track of the elusive Sudbury impact: geochemical evidence for a chondrite or comet bolide. *Terra Nova* **27**, 9–20.

Petrus J. A., Kenny G. G., Ayer J. A., Lightfoot P. C. and Kamber B. S. (2015b) Uranium–lead zircon systematics in the Sudbury impact crater-fill: implications for target lithologies and crater evolution. *J. Geol. Soc. London* **173**, 59–75.

Pfänder J. A., Münker C., Stracke A. and Mezger K. (2007) Nb/Ta and Zr/Hf in ocean island basalts—implications for crust–mantle differentiation and the fate of Niobium. *Earth Planet. Sci. Lett.* **254**, 158–172.

Pickering K. T., Hiscott R. N. and Hein F. J. (1989) *Deep-Marine Environments: Clastic Sedimentation and Tectonics*. Allen and Unwin, Australia.

Planavsky N., Bekker A., Rouxel O. J., Kamber B. S., Hofmann A., Knudsen A. and Lyons T. W. (2010) Rare Earth Element and yttrium compositions of Archean and Paleoproterozoic Fe formations revisited: new perspectives on the significance and mechanisms of deposition. *Geochim. Cosmochim. Acta* **74**, 6387–6405.

Pope K. O., Kieffer S. W. and Ames D. E. (2004) Empirical and theoretical comparisons of the Chicxulub and Sudbury impact structures. *Meteorit. Planet. Sci.* **39**, 97–116.

Prevec S. A., Lightfoot P. C. and Keays R. R. (2000) Evolution of the sublayer of the Sudbury Igneous Complex: geochemical, Sm–Nd isotopic and petrologic evidence. *Lithos* **51**, 271–292.

Richards F. (1975) The Cariaco Basin(trench). *Oceanogr. Mar. Biol. Annu. Rev.* **13**, 11–67.

Rousell D. (1984) Onwatin and Chelmsford formations. In *The Geology and Ore Deposits of the Sudbury Structure*, 1 (eds. E. G. Pye, A. J. Naldrett and P. E. Giblin), pp. 211–218. Ontario Geological Survey, Special.

Rousell D. and Brown G. (2009) *A Field Guide to the Geology of Sudbury, Ontario* Ontario Geological Survey, Open File Report 6243, p. 200.

Rousell D. H. and Long D. G. F. (1998) Are outliers of the Huronian Supergroup preserved in structures associated with the collapse of the Sudbury impact crater? *J. Geol.* **106**, 407–420.

Rudnick R. L. and Fountain D. M. (1995) Nature and composition of the continental crust: a lower crustal perspective. *Rev. Geophys.* **33**, 267–309.

Russell M. J., Hall A. J. and Martin W. (2010) Serpentinization as a source of energy at the origin of life. *Geobiology* **8**, 355–371.

Scott C., Lyons T. W., Bekker A., Shen Y., Poulton S. W., Chu X. and Anbar A. D. (2008) Tracing the stepwise oxygenation of the Proterozoic ocean. *Nature* **452**, 456–459.

Shanks W. S. and Schwerdtner W. M. (1991) Erratum: Crude quantitative estimates of the original northwest–southeast dimension of the Sudbury Structure, south-central Canadian Shield. *Can. J. Earth Sci.* **29**(1991), 835.

Sharp Z. D. and Draper D. S. (2013) The chlorine abundance of Earth: implications for a habitable planet. *Earth Planet. Sci. Lett.* **369–370**, 71–77.

Sheridan M. F. and Wohletz K. H. (1983) Hydrovolcanism: basic considerations and review. *J. Volcanol. Geoth. Res.* **17**, 1–29.

Sleep N. H., Zahnle K. J., Kasting J. F. and Morowitz H. J. (1989) Annihilation of ecosystems by large asteroid impacts on the early Earth. *Nature* **342**, 139–142.

Speers E. C. (1957) The age relation and origin of common Sudbury breccia. *J. Geol.* **65**, 497–514.

Spudis P. D., Martin D. J. P. and Kramer G. (2014) Geology and composition of the Orientale Basin impact melt sheet. *J. Geophys. Res. Planets* **119**, 19–29. http://dx.doi.org/10.1002/2013JE004521.

Stöffler D., Artemieva N. A., Wünnemann K., Reimold W. U., Jacob J., Hansen B. K. and Summerson I. A. T. (2013) Ries crater and suevite revisited-observations and modeling Part I: observations. *Meteorit. Planet. Sci.* **48**, 515–589.

Stüeken E., Anderson R., Bowman J., Brazelton W., Colangelo-Lillis J., Goldman A., Som S. and Baross J. (2013) Did life originate from a global chemical reactor? *Geobiology* **11**, 101–126.

Taylor S. R. and McLennan S. M. (1985) *The Continental Crust; Its Composition and Evolution; An Examination of the Geochemical Record Preserved in Sedimentary Rocks*. Blackwell, Oxford.

Therriault A. M., Fowler A. D. and Grieve R. A. F. (2002) The Sudbury Igneous Complex: a differentiated impact melt sheet. *Econ. Geol.* **97**, 1521–1540.

Thomson J. E. (1960) On the origin of algal-like forms and carbon in the Sudbury Basin, Ontario. *Trans. R. Soc. Canada* **54**, 65–75.

Valley J. W., Peck W. H., King E. M. and Wilde S. A. (2002) A cool early Earth. *Geology* **30**, 351–354.

Verma S. P. (1992) Seawater alteration effects on REE, K, Rb, Cs, Sr, U, Th, Pb and Sr–Nd–Pb isotope systematics of Mid-Ocean Ridge Basalt. *Geochem. J.* **26**, 159–177.

Whitehead R. E. S., Davies J. F. and Goodfellow W. D. (1990) Isotopic evidence for hydrothermal discharge into anoxic seawater, Sudbury basin, Ontario, Canada. *Chem. Geol. Isot. Geosci.* **86**, 49–63.

Williams H. (1957) *Glowing Avalanche Deposits of the Sudbury Basin*, Ontario Dept. of Mines 65th Annual Report, pp. 57–89.

Wohletz K. H. (1983) Mechanisms of hydrovolcanic pyroclast formation: grain-size, scanning electron microscopy, and experimental studies. *J. Volcanol. Geoth. Res.* **17**, 31–63.

Workman R. K. and Hart S. R. (2005) Major and trace element composition of the depleted MORB mantle (DMM). *Earth Planet. Sci. Lett.* **231**, 53–72.

Wright A. J., Parnell J. and Ames D. E. (2010) Carbon spherules in Ni–Cu–PGE sulphide deposits in the Sudbury impact structure, Canada. *Precambrian Res.* **177**, 23–38.

Xu L., Lehmann B., Mao J., Nägler T. F., Neubert N., Böttcher M. E. and Escher P. (2012) Mo isotope and trace element patterns of Lower Cambrian black shales in South China: Multi-proxy constraints on the paleoenvironment. *Chem. Geol.* **318–319**, 45–59.

Associate editor: Christian Koeberl